catalysts

MDPI

Article

Porous Hexacyanometallate(III) Complexes as Catalysts in the Ring-Opening Copolymerization of CO_2 and Propylene Oxide

Guillermo Penche, Juan R. González-Velasco and M. Pilar González-Marcos *

Chemical Technologies for Environmental Sustainability Group, Department of Chemical Engineering, Faculty of Science and Technology, University of the Basque Country UPV/EHU, P.O. Box 644, E-48080 Bilbao, Spain; guillermo.penche@ehu.eus (G.P.); juanra.gonzalezvelasco@ehu.eus (J.R.G.-V.)
* Correspondence: mp.gonzalezmarcos@ehu.eus

Abstract: In this work, six porous hexacyanometallate complexes ($Ni_3[Co(CN)_6]_2$, $Co_3[Co(CN)_6]_2$, $Fe_3[Co(CN)_6]_2$, $Ni_3[Fe(CN)_6]_2$, $Co_3[Fe(CN)_6]_2$, $Fe_4[Fe(CN)_6]_2$) were synthesized by a complexing agent assisted coprecipitation method and thoroughly characterized via X-ray diffraction (XRD), Fourier-transform infrared spectroscopy (FT-IR), thermogravimetric analysis (TGA), in situ high-temperature X-ray diffraction (HT-XRD), elemental analysis (EA), X-ray fluorescence (XRF), scanning electron microscopy (SEM), transmission electron microscopy (TEM), N_2 physisorption, and gas–solid phase titration with NH_3. The thermal stability, chemical composition, pore size and volume, crystallite size and density of surface acid sites were strongly sensitive to both the transition metal and the cyanometallate anion employed. On that basis, transition metal hexacyanometallates must be perceived as an adaptable class of zeolite-like microporous materials. The catalytic properties of these compounds were tested by copolymerization of propylene oxide and CO_2, a green route to obtain biodegradable aliphatic polycarbonates. All compounds under study showed moderate activity in the target reaction. The obtained copolymers were characterized by modest CO_2 content (carbonate units ranging from 16 to 33%), random structure ($R_{PEC} \approx 70\%$), and moderate molecular weight (M_w = 6000–85,400 g/mol) with broad dispersity values ($Đ_M$ = 4.1–15.8).

Keywords: microporous materials; zeolite-like materials; transition metal hexacyanometallates; CO_2 utilization; copolymerization; biodegradable polymers

Citation: Penche, G.; González-Velasco, J.R.; González-Marcos, M.P. Porous Hexacyanometallate(III) Complexes as Catalysts in the Ring-Opening Copolymerization of CO_2 and Propylene Oxide. *Catalysts* **2021**, *11*, 1450. https://doi.org/10.3390/catal11121450

Academic Editor: Hamidreza Arandiyan

Received: 1 November 2021
Accepted: 24 November 2021
Published: 29 November 2021

1. Introduction

Transition metal cyanometallates (also known as Prussian blue analogues, double metal cyanides, cyanometallates, or cyano metal complexes) are a class of inorganic coordination polymers (CPs) that result from the assembly of cyanometallate anions ($[M(CN)_a]^{b-}$) via nitrogen-bound transition metal cations (T^{c+}) [1–4]. Their general molecular formula is $T_b[M(CN)_a]_c$, where T and M represent the outer and inner transition metal cations, respectively. The crystal structure of this family of compounds is subject to the coordination number and geometry of the nodes (outer transition metal cations) and connectors (cyanometallate anions). Based on this, lattice structures of one [5–7], two [8–10], or three [11] dimensions can be assembled, offering a wide range of potential applications. Historically, transition metal cyanometallates have been used as pigments or dyestuffs [12,13]. However, they have recently received increased interest by the scientific community due to their photo-magnetic [14,15] ferromagnetic [16,17] optical [18], ion-sensing [19,20], electrochemical [21,22], gas storage [23–26], ion-exchange [27], catalytic [28], and other properties.

In the field of catalysis, transition metal cyanometallates have been proven to be active in esterification [29,30], transesterification [31], hydrolysis [32], addition [33], coupling [34], oxidation [35], and ring-opening reactions [36–40]. Their catalytic activity is associated with the presence of so-called coordinatively unsaturated metal sites (CUMSs), analogous to those present in the active catalysts of metal–organic frameworks (MOFs), on their lattice [41]. It should be noted that inner transition metal cations in cyanometallate

anions have their coordination sphere fully filled with the carbon atoms of the cyanide groups. Thus, the inner transition metal offers no free coordination centers and CUMSs are consequently ascribed uniquely to outer transition metal centers.

Transition metal cyanometallates are usually obtained from a precipitation reaction between aqueous solutions of water-soluble transition metal salt and metal cyanide salt. When these complexes are intended for catalytic purposes, some changes in the synthesis procedure are usually made in order to increase their catalytic activity. In practice, an excess of the transition metal precursor salt is used along with organic additives such as complexing agents (CAs) and sometimes even co-complexing agents (co-CAs). These modifications cause important changes to the physicochemical properties of cyanometallates. The degree of crystallinity is severely reduced [42] and smaller particles are formed [43]. On occasion, new solid phases also appear, generally phases with no long-range order or completely amorphous phases. All of this results in an increased number of defects, which in turn leads to increased CUMS density and accessibility.

Even though transition metal cyanometallates have been demonstrated to possess very promising catalytic properties, their scope as catalytic materials has hardly been explored until now. One of the most promising processes involving these compounds as catalysts is the copolymerization of CO_2 and epoxides to produce aliphatic polycarbonates (Figure 1). The copolymerization of CO_2 and propylene oxide (PO) is especially relevant, since the polycarbonate thus obtained, polypropylene carbonate (PPC), exhibits excellent biodegradable/biocompatible properties. The catalytic copolymerization of CO_2 and epoxides constitutes a technology that combines numerous economic and environmental advantages. From the economic point of view, the use of an inexpensive and naturally abundant raw material such as CO_2 translates into reduced cost compared with conventional epoxide homopolymers [44]. From an environmental perspective, this technology involves long-term CO_2 storage and replaces oil-based monomers with a renewable molecule [45]. A life-cycle assessment study concluded that partial substitution of epoxides with CO_2 reduces greenhouse gas emission by approximately 11–19% and fossil resource utilization by approximately 13–16% [46]. A broad range of zinc-based hexacyanometallates ($Zn_b[M(CN)_6]_c$) has been screened for the copolymerization of CO_2 and epoxides [37,38,47–52]. All of them share some common disadvantages: (i) they require high pressure and long reaction time to obtain an appreciable incorporation of CO_2 into the polymer backbone [53,54], (ii) they produce a considerable amount of cyclic carbonate byproducts [55], and (iii) they lead to low-molecular-weight polymers [53]. For that reason, research on the application of transition metal cyanides in CO_2/epoxide copolymerization is moving toward a search for novel alternative complexes [56,57].

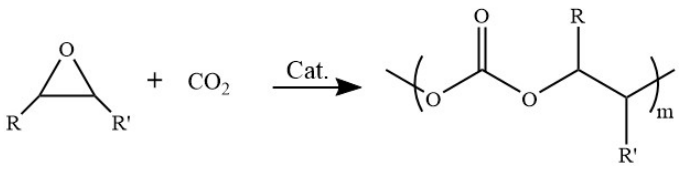

Figure 1. Copolymerization of CO_2 and epoxides.

Within transition metal cyanometallates, those based on divalent transition-metal cations (T^{2+}) and trianionic hexacyanometallates ($[M(CN)_6]^{3-}$) represent an attractive group of 3-D porous materials. When the outer transition metal cation adopts an octahedral coordination, these solids crystallize in an open microporous structure built from face-centered cubic unit cells (Figure 2a). Divalent transition metal hexacyanometallates(III) themselves do not respect the oxidation state sum rule. Thus, compliance with that rule is conditional on vacancies at 33% of the $[M(CN)_6]^{3-}$ sites. These vacancies lead to a unique pore network composed of vacancy voids (effective diameter of ca. 10 Å) interconnected through tiny non-vacancy windows of approximately 5 Å in diameter [58]. Moreover, every missing $[M(CN)_6]^{3-}$ block provides eight bare T metal sites per unit cell [59]. In other

words, vacancies afford bulk CUMSs inherent to the structure. Normally, water molecules complete the coordination sphere of these bare-metal sites after synthesis (Figure 2b). Due to their high surface area, bulk microporosity, and content in open metal sites, divalent transition metal cyanometallates are ideal candidates for separation and storage of small gaseous molecules and catalytic applications [60–62].

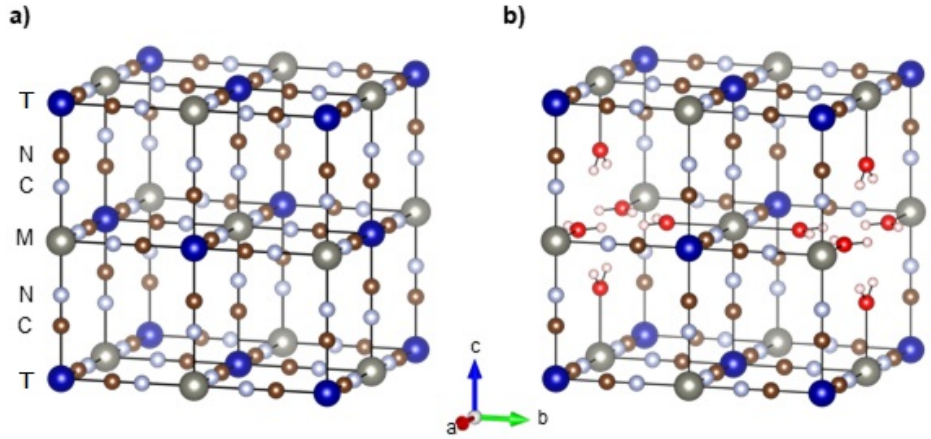

Figure 2. Crystal structure of divalent transition metal hexacyanometallate(III) compounds (**a**) without and (**b**) with $[M(CN)_6]^{3-}$ vacancies.

Herein, six isostructural zeolite-like divalent transition metal hexacyanometallates(III) were synthesized by combining three distinct outer transition metal cations (T = Ni^{2+}, Co^{2+}, and Fe^{2+}) with two hexacyanometallate(III) anions $[M(CN)_6]^{3-}$, M = Co^{3+} and Fe^{3+}); they are abbreviated as T-M in reference to the outer (T) and inner (M) transition metal cations that comprise them. Complexes were prepared through a coprecipitation method employing *tert*-butyl alcohol (TBA) as CA during the synthesis. Physicochemical properties were analyzed in depth and correlated with the T-M metal combination. In addition, we further investigated the catalytic behavior of these hexacyanometallate complexes in the copolymerization of CO_2 and found all of them to be catalytically active. We hope that this work will boost studies on the application of these outstanding porous materials in catalysis and related fields.

2. Results

2.1. Porous Hexacyanometallates(III) Characterization

2.1.1. Crystal and Electronic Structure

IR spectroscopy is an enormously powerful tool for identifying the coordination environment of cyano groups in cyanometallates. Cyanide ligands have an ambidentate nature and can act as σ donors as well as π acceptors. Free cyanide ion (CN^-) exhibits a ν(C≡N) band at 2080 cm^{-1} (aqueous solution) [63]. Monodentate cyanide ligands are bound to a metal through carbon atoms via σ-bond, donating electrons to the metal, and π-bond, accepting electrons from the metal. Since electrons are removed from the weakly antibonding 5σ orbital, σ-donation causes an increase in the frequency of ν(C≡N), whereas π-backbonding contributes to a decrease, due to the entry of electrons into the 2pπ* antibonding orbital. As CN ligand is a better σ-donor than π-acceptor, the ν(C≡N) frequency for terminal M-C≡N complexes is higher than that of free CN^- ion [63]. In bridged M-C≡N-T cyano complexes, the ν(C≡N) band normally shifts to higher frequencies as a consequence of an increased C≡N force constant due to the donation of nitrogen lone pair electrons to the outer transition metal cation [64].

The FT-IR spectra of the studied series of porous hexacyanometallates(III) are shown in Figure 3. Table 1 summarizes the frequencies at which the bands of interest manifested in the hexacyanometallate(III) compounds and their precursors. In line with

theoretical studies, bands in the low-frequency region were assigned in the following order: ν(M-C) > δ(M-CN) [65]. The δ(Co-CN) band in cyanocobaltates usually falls below 400 cm^{-1} [66]. In addition to the adsorption bands related to the octahedral $[M(CN)_6]$ block, there are motions related to the vibration of water molecules: two in the ν(OH) region, due to coordinated (sharp) and hydrogen-bonded (broad) water molecules and the δ(HOH) band around 1610 cm^{-1}. Motions associated with the presence of TBA were not detected.

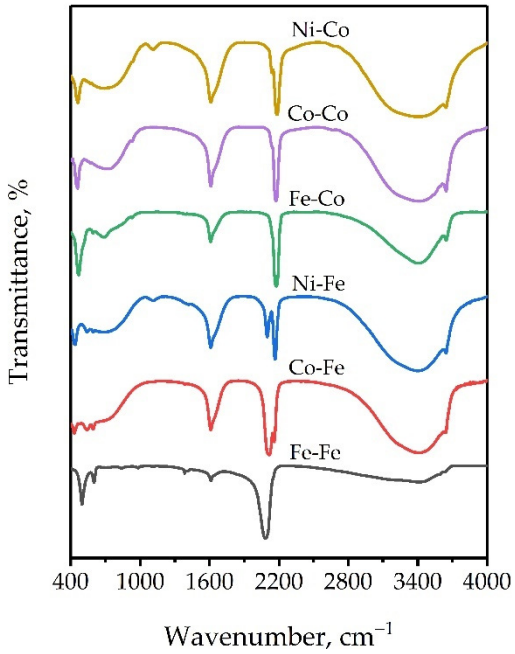

Figure 3. FT-IR spectra for the studied porous hexacyanometallates(III).

Table 1. Frequency (in cm^{-1}) of FT-IR adsorption bands of studied porous hexacyanometallates(III).

Compound	δ(M^{II}-CN)	ν(M^{II}-C)	ν(CN)	δ(HOH)	ν(H_2O)
$[Co(CN)_6]^{3-}$	416 s	565 m	2125 s	-	-
$[Fe(CN)_6]^{3-}$	417 m	511 m, 583 w	2118 s	-	-
Ni-Co	-	461 m	2141 m, 2183 s	1609; 1634 (sh)	3404; 3646 (br, s)
Co-Co	-	457 m	2176 s	1609; 1634 (sh)	3409; 3646 (br, s)
Fe-Co	-	469 m	2175 s	1607; 1639 (sh)	3415; 3646 (br, s)
Ni-Fe	432 sh, 439 w	541 w, 594 w	2098 m, 2167 s	1609; 1662 (sh)	3396; 3646 (br, s)
Co-Fe	431 w, 440 sh	540 w, 593 w	2116 s, 2159 m	1609; 1651 (sh)	3404;3641 (br, s)
Fe-Fe	501 m, 512 sh	603 w	2080 s	1606; 1638 (sh)	3369; 3595; 3625 (br, br, s)

s, strong; m, medium; w, weak; sh, shoulder, br, broad.

Apart from the Fe-Fe compound, which will be discussed below, the ν(C≡N) bands of the synthesized hexacyanometallates(III) were located at higher wavenumbers than those of their linear precursors. These results prove the success of the synthesis procedure in the formation of cyanide-bridged bimetallic structures. In some of the complexes, two or more different vibration bands can be observed in both the ν(C≡N) region and the low-frequency region. This co-existence of bands can be attributed to multiple phenomena: the presence of precursor remains, linkage isomerism [67], electron transfer from M to T [68], partial reduction of the M metal [69], structural distortions [70], or surface cyanide groups [71].

The Fe-Fe compound shows the ν(C≡N) band at 2080 cm^{-1}, which falls below the stretch vibration of its monodentate precursor. A peak at that frequency should belong to a

ν(Fe^{2+}-C≡N-Fe^{3+}) mode rather than the expected ν(Fe^{3+}-C≡N-Fe^{2+}) [72]. When Fe^{2+} acts as the inner transition metal, owing to its lower oxidation number, it reduces the σ-donation from the CN^- group and thus weakens the CN bond and lowers ν(C≡N). Accordingly, the ν(C≡N) band frequency indicates that the prepared compound is indeed the well-known Prussian blue complex ($Fe_4{}^{3+}[Fe^{2+}(CN)_6]_3$). The transition from the $Fe_3[Fe(CN)_6]_2$ to $Fe_4[Fe(CN)_6]_3$ configuration when the precipitation reaction between solutions of an Fe^{2+} salt and an $[Fe^{3+}(CN)_6]^{3-}$ salt is carried out has already been reported [73]. According to Ito et al., this fact can be explained by: (i) a charge transfer from high-spin Fe^{3+} to low-spin Fe^{2+} or (ii) a 180° turn of the CN^- ligand during the combining of precursors in the precipitation reaction [74].

The ν(C≡N) mode in cyano-bridged compounds is mainly governed by the interaction force with the inner transition metal cation, which in turn depends on: (i) the electronegativity, (ii) the oxidation state, and (iii) the coordination number of the cation [75]. Given that Co^{3+} cation has far higher electronegativity than Fe^{3+} cation, σ-donation from cyanide is stronger in T-Co than in T-Fe complexes. Consequently, the ν(C≡N) values of T-Co complexes are expected to be higher than those of T-Fe compounds, and this was fulfilled in the synthesized materials. In addition, the ν(C≡N) vibration has also demonstrated sensitivity to the nature of the outer transition metal cation. The frequency values for the ν(C≡N) bands of the samples are in decreasing order of Ni^{2+} > Co^{2+} > Fe^{2+}, which matches perfectly with the electronegativity of the metals [76]. From these results, one can deduce that increased electronegativity of the outer transition metal leads to promoted electron donation from the N atom of the cyanide ligand.

XRD is also a fundamental technique for structural characterization of hexacyanometallates. Figure 4 shows the diffractograms of the studied complexes. All patterns are identical, which reflects that all hexacyanometallate(III) compounds crystallized with the same unit cell. The patterns are indexed to a cubic lattice structure with space group Fm-3m (major peaks located at 2θ around 14.9°, 17.5°, 24.9°, 35.4°, and 39.7°) [77]. Peak widths reveal a lack of long-range order in the crystal lattices of samples. More crystallographic details of the synthesized compounds are listed in Table 2.

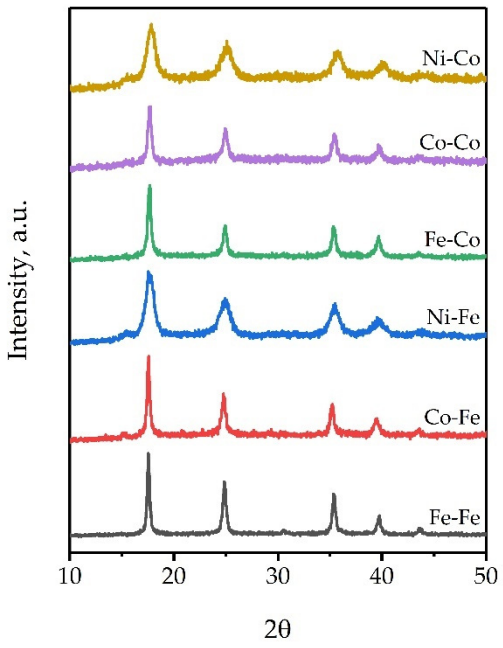

Figure 4. XRD spectra for the studied porous hexacyanometallates(III).

Table 2. Unit cell edge length, cell volume, crystallite size, and strain value for the studied porous hexacyanometallates(III).

Compound	Cell Edge (Å)	V (Å^3)	Crystallite Size (nm)		Strain (ε)
			D-S	W-H	
Ni-Co	10.07	1020	9.4	13.2	0.00220
Co-Co	10.16	1049	21.5	29.4	0.00093
Fe-Co	10.17	1051	26.2	33.5	0.00061
Ni-Fe	10.15	1047	8.3	11.4	0.00243
Co-Fe	10.22	1068	27.6	43.6	0.00103
Fe-Fe	10.16	1049	34.6	44.1	0.00049

Coherent domain size was estimated from the Debye–Scherrer (D-S) equation [78], applied to the most intense diffraction peak, and the Williamson–Hall (W-H) method [79]. The W-H method takes into consideration peak broadening due to the lattice strain produced by crystal imperfections (vacancies, dislocations, grain boundaries, and so on). It should be kept in mind that the divalent transition metal hexacyanometallate(III) structure is inherently disordered owing to randomly distributed vacant sites. Further, the use of TBA and excess TCl_2 salt during the synthesis was expected to partially collapse the crystal structure of the studied compounds. Thus, the W-H method was considered a more accurate procedure for determining the crystallite size of the samples. The W-H plots are provided in the Supplementary Materials (Figure S1). The W-H method supplies crystallite sizes between 25 and 60% larger than those obtained from the Scherrer equation, which indicates the magnitude of the crystal defects. The coherent domain size of the samples decreased with the electronegativity of the outer transition metal cation in the order $Fe^{2+} > Co^{2+} > Ni^{2+}$. In other words, crystallite size proved to be modulated by the outer metal cation used. At the same time, the strain values seemed to be dominated by crystallite size.

The unit cell edge length for the cubic phases was estimated according to the position of the peak corresponding to the plane (110). For T-Co complexes, cell edges obeyed the same trend as the coherent domain size; they diminished with the electronegativity of the outer transition metal cation. Since the cell edge is determined by the length of the T-N≡C-Co-C≡N-T chain, its value will depend on the interaction strength between the outer and inner metal through the C≡N bridges [80]. FT-IR results show that the higher the electronegativity of the outer transition metal cation, the greater the donation from the cyanide ligand. Given that electron donation from cyanide ligand to metal cations strengthens their interaction, cell edge length should agree with the frequency of the ν(C≡N) band observed via FT-IR. Indeed, a linear relationship between these parameters for T-Co compounds was observed (Figure S2). This relationship was also true for the Ni-Fe and Co-Fe samples. However, the Fe-Fe compound cannot be compared because of the change in the oxidation state of the involved metals. Except for the latter, cell edges of T-Co compounds were smaller than those of T-Fe compounds, which demonstrates how electron donation to inner transition metal also determines the cell edge value. The importance of these results should not be overlooked, because pore size and volume will ultimately depend on the edge length of the unit cell. That is to say, porosity of these kinds of zeolitic materials can be easily tuned by the combination of inner and outer transition metal cations.

2.1.2. Thermal Stability, Degree of Hydration, and Dehydration Process

The thermal behavior of porous hexacyanometallate(III) compounds was studied by TGA in oxidizing and inert atmospheres (Figure 5). Analyzing the evolved gases (not displayed) during TGA allowed us to correlate the weight loss stages with their corresponding thermal process. Basically, two major stages of weight loss could be distinguished in the TG curves of the samples: (i) 25–200 °C due to the loss of water molecules and (ii) ≥300 °C due to decomposition. Table 3 summarizes the degree of hydration, the dehydration tempera-

ture, and the decomposition temperature of the samples. Porous hexacyanometallates(III) have two kinds of water species: (i) zeolitic water confined in the porous cavities and (ii) coordinated water attached to bare T metals. Upon heating, coordinated and non-coordinated water losses overlap, resulting in a single weight loss step with no appreciable intermediate inflections. The dehydration temperature was slightly higher in the oxidizing atmosphere, probably due to the intake of water from the environment slowing down the dehydration process. Inner transition metal cation did not seem to significantly affect the dehydration temperature. However, the dehydration temperature followed an upward trend with the electronegativity of the outer transition metal cation. This trend indicates a strengthening of the T-OH_2 interaction with the electronegativity of the outer transition metal cation. As with IR spectroscopy, the discharge of TBA could not be identified in any of the synthesized complexes (absence of molecular ion $C_4H_{10}O^+$ (m/z = 74)).

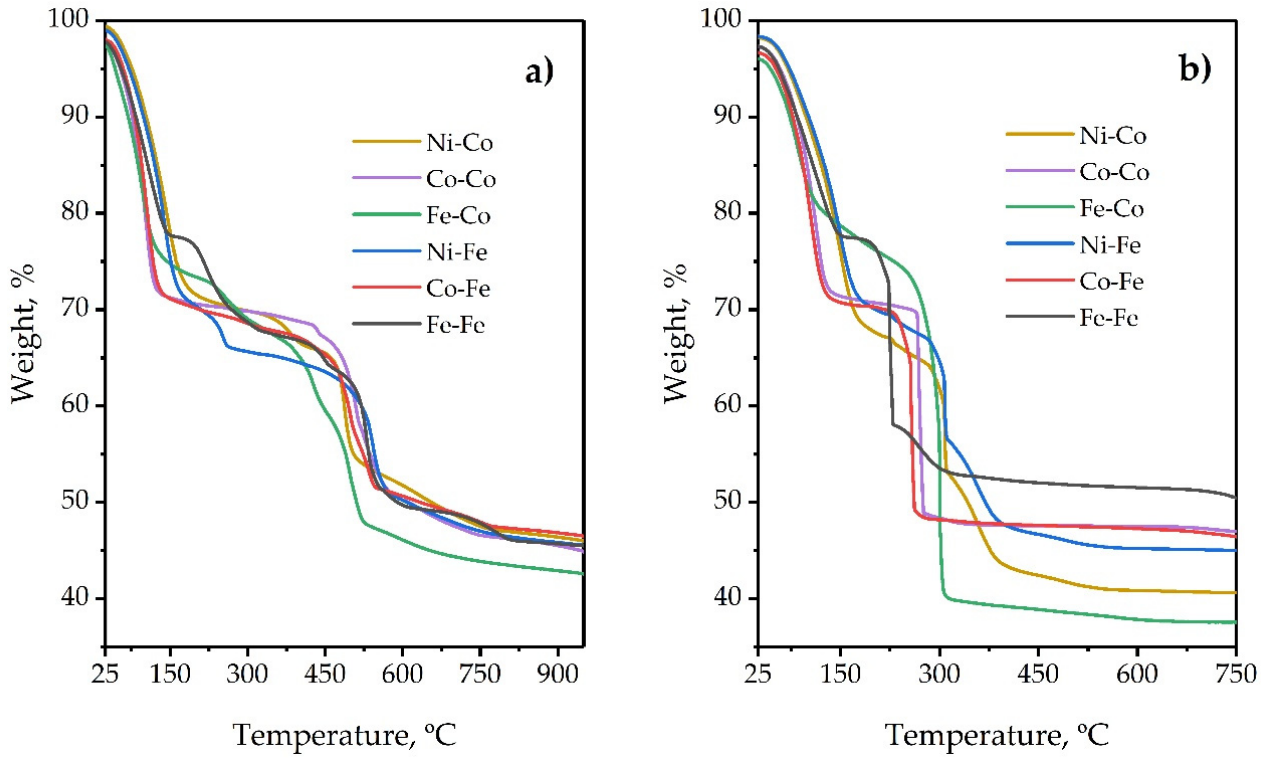

Figure 5. TG curves of the studied porous hexacyanometallates(III) in (**a**) inert atmosphere and (**b**) oxidizing atmosphere.

Table 3. Degree of hydration, dehydration temperature, and decomposition temperature of the studied porous hexacyanometallates(III).

Compound	H_2O, wt %	Dehydration Temp. (°C) *		Decomposition Temp. (°C) *	
		N_2	Air	N_2	Air
Ni-Co	29.30	145	150	490	310
Co-Co	29.71	110	115	515	265
Fe-Co	25.15	94	96	495	290
Ni-Fe	29.73	140	150	540	305
Co-Fe	30.83	105	108	500	255
Fe-Fe	22.46	107	110	525	225

* Temperature of maximum weight loss.

The decomposition stage was much more abrupt and shifted to a lower temperature in the oxidizing atmosphere than in the inert stage. Thermolysis in air was mainly accompanied by the liberation of CO_2 (m/z = 44), a product of the oxidation of CN

bridges. Thermolysis in N_2 consisted of multistage mass loss characterized by the release of cyanide ligands as cyanogen (C_2N_2; molecular ions detected by EGA: CN^+ (m/z = 26) and $C_2N_2^+$ (m/z = 52)) and hydrogen cyanide (HCN; molecular ions detected by EGA: HCN^+ (m/z = 27)). It is worth noting that the Fe-Co, Ni-Fe, and Fe-Fe samples showed partial decomposition in the range of 150–300 °C, which could be confused with a loss of TBA or coordinated water. Notwithstanding, this intermediate weight loss step was accompanied by the liberation of CO_2 and C_2N_2, so it must be attributed to decomposition of the tiniest hexacyanometallate(III) particles.

The porous framework of hexacyanometallates(III) has proven to be flexible, i.e., it contracts and distorts upon dehydration and recovers when rehydrated. Here, we analyzed the effect of the dehydration process on the crystalline structure of porous hexacyanometallates(III) via HTXRD in an oxidizing atmosphere. The dehydration process led to a distortion of the structure marked by a gradual decrease in peak intensity at 2θ = 24.9° (220) and 35.4° (400), until they disappeared. Remarkably, the peak around 17.5° (200) remained in all samples, reflecting that the cubic structure maintained part of its identity (Figure S3). Unit cell edge length decreased upon dehydration, proving the structural flexibility of porous hexacyanometallates(III). Table 4 summarizes the cell contraction and volume reduction of the studied compounds upon dehydration. No changes were appreciated in peak broadening. The stability of the crystal structure was also intended to be studied in vacuum conditions (2–3 Pa); however, the structures collapsed immediately when the pressure dropped, indicating rapid and almost complete dehydration of the samples under high vacuum conditions even at room temperature. Notably, we were able to check that the crystal structure of the studied compounds returned to its original state after one night of exposure to the atmosphere, showing the reversibility of the process.

Table 4. Effect of dehydration over hexacyanometallate(III) cell dimensions.

Compound	Cell Contraction (%)	Cell Edge after Dehydration (Å)	Cell Volume Reduction (%)	Cell Volume after Dehydration ($Å^3$)
Ni-Co	1.7	9.89	5.1	968
Co-Co	2.0	9.96	5.7	989
Fe-Co	1.2	10.05	3.5	1015
Ni-Fe	1.8	9.97	5.4	991
Co-Fe	2.4	9.98	7.0	993
Fe-Fe	1.4	10.02	4.1	1006

2.1.3. Chemical Composition

The chemical composition of the studied porous hexacyanometallates(III) was analyzed by XRF, EA, and TGA, and the results are summarized in Table 5. Note that the general formula could not be assessed for those complexes whose outer and inner metals were the same. For the rest of the samples, the content of T per M atom determined by XRF was higher than 1.5, which is the stoichiometric value. Remarkably, the T/M atomic ratio showed a strong correlation with the size of the crystallite (Figure S4). If the building blocks of $[M(CN)_6]^{3-}$ remain unmodified in the final structure of the hexacyanometallate(III) complex, the surface must be constituted by M-C≡N endings or bare T metals. A smaller crystallite size means a higher surface-to-volume ratio, and consequently a higher concentration of bare T metals exposed at the surface.

Table 5. Chemical composition of the studied porous hexacyanometallates(III).

Compound	XRF (wt%)				T/M (at./at.)	EA (wt%)		Estimated Catalyst Formulation
	T	M	K	Cl		C	N	
Ni-Co	24.5	12.3	0.2	1.9	2.0	14.4	17.6	$Ni_{1.99}[Co(CN)_{6.01}]\cdot 7.78\ H_2O$ *$\cdot 0.26\ Cl^-\cdot 0.03\ K^+$
Co-Co	M^I=M^{II}: 38.3		0.4	1.8	-	14.4	16.2	-
Fe-Co	21.8	12.8	0.1	1.4	1.8	17.3	20.1	$Fe_{1.81}[Co(CN)_{6.45}]\cdot 6.41H_2O$ *$\cdot 0.19\ Cl^-\cdot 0.01\ K^+$
Ni-Fe	24.8	11.8	0.2	1.5	2.0	14.3	17.8	$Ni_{2.01}[Fe(CN)_{6.02}]\cdot 7.80\ H_2O$ *$\cdot 0.19\ Cl^-\cdot 0.02\ K^+$
Co-Fe	23.5	13.0	0.6	1.1	1.7	15.5	17.3	$Co_{1.72}[Fe(CN)_{5.30}]\cdot 6.95\ H_2O$ *$\cdot 0.14\ Cl^-\cdot 0.06\ K^+$
Fe-Fe	M^I=M^{II}: 36.6		1.5	0.9	-	16.8	19.6	-

* Water content determined from TGA curves.

All samples had a certain content of chlorine and potassium originating from the precursors TCl_2 and $K_3[M(CN)_6]$. The presence of chlorine in transition metal cyanometallates has been shown to be critical in order to obtain highly active catalysts in both epoxide homopolymerization and CO_2/epoxide copolymerization [42,71,81]. Chlorine is deemed to be incorporated into the lattice of cyanometallates as dissociated Cl^- giving rise to C≡N-T-Cl terminations, which are proposed as dormant active sites [42]. The potassium content was almost negligible in the synthesized complexes; only the Fe-Fe sample showed content greater than 1%. Normally, cubic zeolite-like hexacyanometallates(III) present some potassium entrapped in the zeolitic cavities of the cubic framework, which acts as a source of charge-compensator ions. The reason why the Fe-Fe compound had more potassium than the rest could be explained by the aforementioned reduction of the inner metal Fe^{3+} to Fe^{2+}. In parallel studies, we found that divalent transition metal hexacyanometallates(II) present more potassium content than their trianionic counterparts. This is probably due to the greater negative charge of the hexacyanometallate anion in hexacyanometallates(II).

2.1.4. Morphology and Textural Properties

The morphology of the porous hexacyanometallates(III) was further investigated by SEM (Figure 6) and TEM (Figure 7) microscopy. SEM micrographs reveal bulky particles (2–10 μm) built by several smaller grains. The primary particle size distribution (PSD) evaluated by TEM verified that the studied compounds were formed by a conglomerate of nanosized grains. PSD profiles are included in the Supplementary Materials (Figure S5). Notably, grain sizes determined by TEM were quite similar to the crystallite sizes obtained from the line broadening analysis of XRD peaks. This is usually observed when the primary particle size is in the nano range [82]. We assume that this phenomenon emerged as a result of the use of TBA during the synthesis, which must have acted somewhat as a capping agent, preventing uncontrolled growth of the grains. Grain sizes were strongly influenced by the electronegativity of both inner and outer transition metal cations: the higher the electronegativity, the smaller the size.

The textural properties of the dehydrated compounds were studied by N_2 physisorption at 77 K (Figure 8a). Although divalent transition metal hexacyanometallates(III) are microporous materials, some of the studied compounds exhibited hints of mesoporosity. The origin of the mesoporous frame is attributable to the inter-crystalline spaces formed by the aggregation of nanocrystals. In fact, the average pore diameter (d_{meso}) of mesopores was in the range of grain sizes extracted from TEM micrographs (Figure 8b). Inter-crystalline mesoporosity led to a significant increment of the catalysts' external surface area (S_{ext}). Table 6 lists the contributions of micropore and open surface area to the synthesized porous hexacyanometallates(III). Due to size and diffusional limitations, the CO_2/PO copolymerization reaction was not expected to take place inside the micropores. Thus, an increment in S_{ext} translates to an increment in the amount of catalytically active

surface area. Ni-Co and Ni-Fe samples barely showed any sign of mesoporosity because of the high level of compaction existing between the tiny particles of these samples, as can be observed in SEM micrographs.

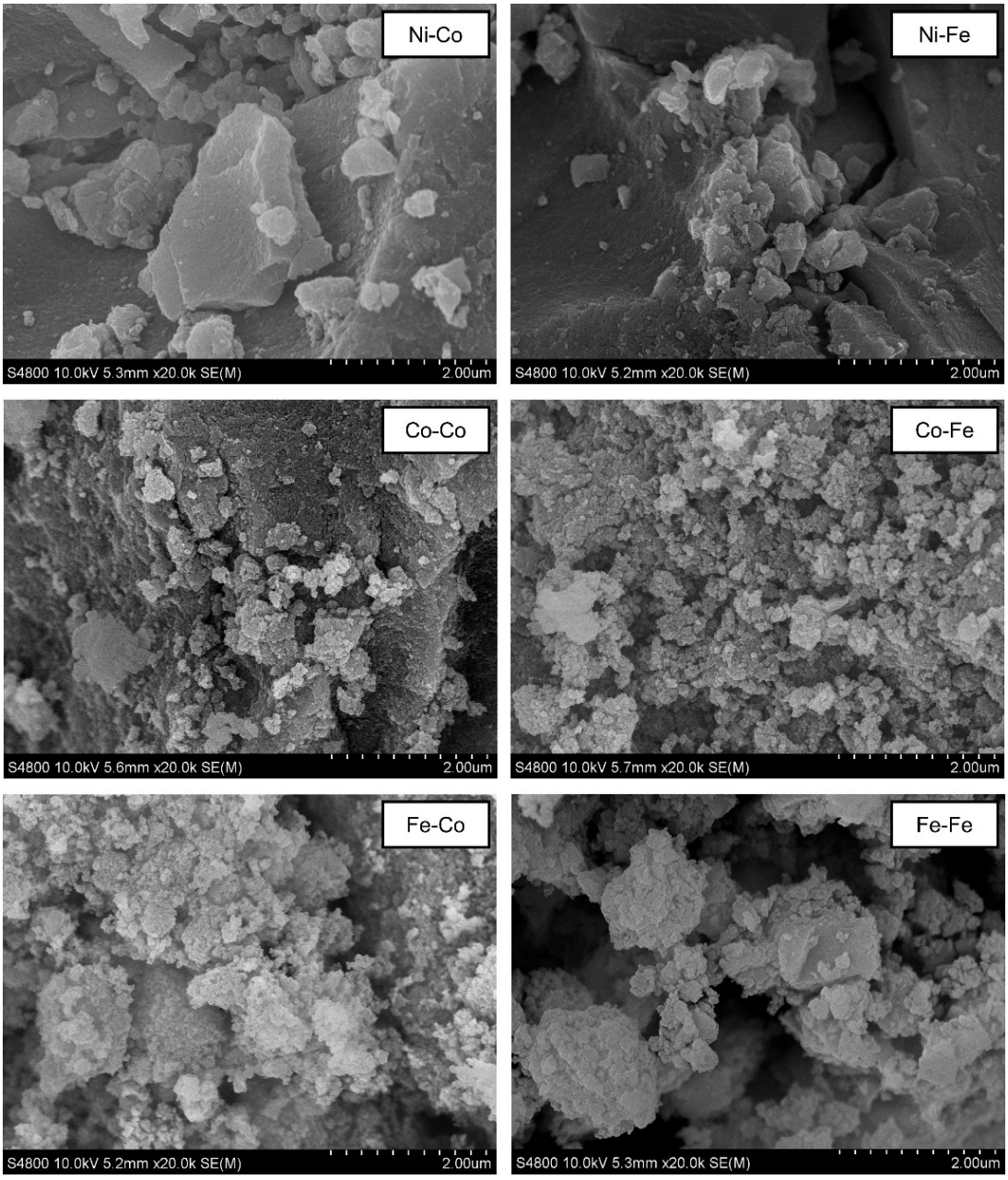

Figure 6. SEM images of the studied porous hexacyanometallates(III).

The micropore capacity (V_{micro}) of the studied compounds was estimated by applying three different approaches (Table 7). There was huge variation when going from one method to another. The Dubinin–Asthakov (D-A) method resulted in the highest V_{micro}, followed by t-plot and Rouquerol. Curiously, the smaller the micropore contribution, the greater the divergence between methods. Thus, it can be stated that determining micropore capacity by the employed methods is affected by the presence of mesoporosity.

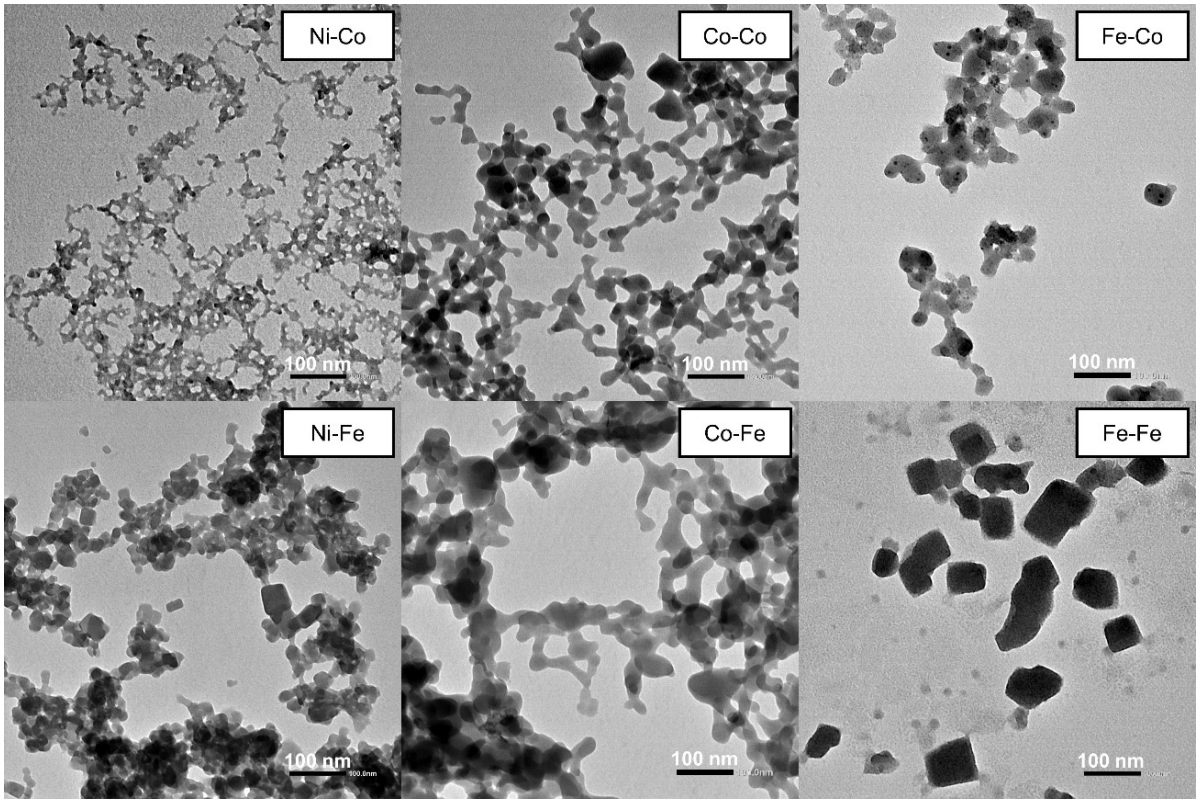

Figure 7. TEM images of the studied porous hexacyanometallates(III).

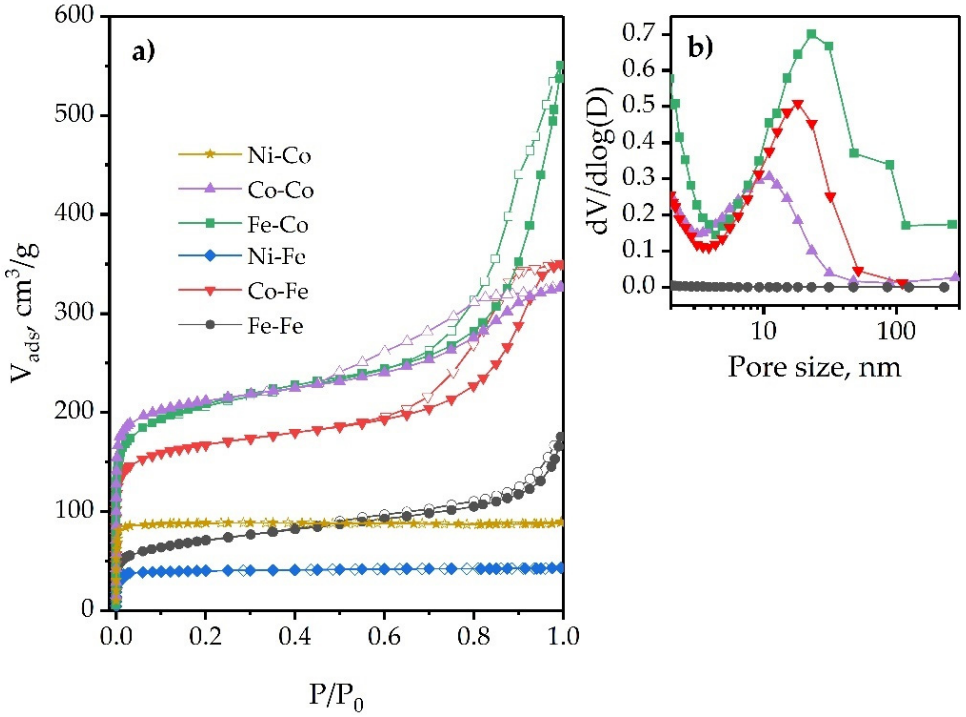

Figure 8. Textural properties of the studied porous hexacyanometallates(II): (**a**) N_2 adsorption-desoprtion isotherms, (**b**) BHJ mesopore size distribution obtained from the adsorption branch.

Table 6. Comparison of total surface area (S_{BET}), external surface (S_{ext}) area, and micropore surface area of hexacyanometallates(III) based on N_2 adsorption data.

Compound	S_{BET} [a] (m^2/g)	S_{ext} [b] (m^2/g)	Surface Area Contributed by Micropores (%)
Ni-Co	373	-	100
Co-Co	801	155	81
Fe-Co	757	156	79
Ni-Fe	161	4	98
Co-Fe	624	95	85
Fe-Fe	213	75	65

[a] Calculated according to the Rouquerol procedure [83]. [b] Determined by t-plot method in the range 6 < t < 9 Å [84].

Table 7. Comparison of total volume (V_t) and micropore volume (V_{micro}) calculated according to different methods from N_2 adsorption data.

Compound	V_t [a] (cm^3/g)	V_{micro} (cm^3/g)			Pore Volume Contributed by Micropores [e] (%)
		$V_{m(BET)} = V_{micro} + V_{m(ext)}$ [b]	DA-Plot [c]	t-Plot [d]	
Ni-Co	0.146	0.132	0.146	0.144	97
Co-Co	0.496	0.230	0.325	0.258	55
Fe-Co	0.680	0.214	0.309	0.263	39
Ni-Fe	0.066	0.056	0.065	0.062	92
Co-Fe	0.590	0.188	0.267	0.216	38
Fe-Fe	0.201	0.049	0.097	0.068	36

[a] Saturation capacity was measured at P/P_0 of 0.95. [b] V_{micro} calculated by extracting non-microporous monolayer obtained from t-method from BET monolayer or BET strong retention capacity [83]. [c] V_{micro} calculated according to D-A method [85]. Values of parameters of D-A equation are included in Supplementary Material (Table S1). [d] V_{micro} calculated according to t-plot method [84]. [e] Based on average micropore volume obtained by three methods.

The Ni-Co and Ni-Fe complexes displayed much lower N_2 uptake than expected based on the amount of water lodged in their porous networks according to TG curves, which indicates that part of the porous framework was inaccessible for N_2. Analogous results have been reported by other authors [80,86]. It is suggested that such behavior responds to a distortion of the structure and subsequent reduction of the effective pore width upon dehydration due to the high polarizing power (or electronegativity) of the Ni^{2+} cation. The Fe-Fe complex porous framework also shows low accessibility for N_2 molecules. This compound has also been reported to be extremely sensitive to the pretreatment process [23]. Moreover, the relatively high potassium content measured by XRF may result in a partial blockage of the pores. Remarkably, other compounds, such as Co-Co, Fe-Co, and Co-Fe, showed high N_2 uptake, indicating that their porous framework remains accessible despite the thermal treatment.

2.1.5. Density of Coordinatively Unsaturated Metal Sites (CUMSs)

The catalytic activity in transition metal cyanometallate catalysts, including porous hexacyanometallates, is ascribed to the aforementioned CUMSs. Given that CUMSs are electron-deficient sites, they cannot but act as Lewis acid sites (LAS). Indeed, cyanometallates are considered to be pure Lewis acid catalysts; that is to say, no Brønsted acid or basic centers have been identified in their structure [87–89]. Thus, knowing the density of acid sites or CUMSs on the surface of these compounds is a key factor in understanding their catalytic properties. Herein, the number of CUMSs was determined through surface acid site titration employing NH_3 as probe molecule. NH_3 is an ideal probe molecule since it is small (kinetic diameter of 2.6 Å) and allows titration of weak acid sites [90]. Total surface acidity was assessed from the net weight gain recorded after an isothermal adsorption step of NH_3 at 100 °C followed by removal of physisorbed molecules with a He stream. The saturation curves of NH_3 adsorption on the different porous hexacyanometallates(III) are

displayed in Figure S6. Unfortunately, NH_3-TPD experiments were considered not suitable to measure the strength of the CUMSs, since some of the studied compounds partially decomposed at temperatures as low as 190 °C in an inert atmosphere (see Figure 5).

Table 8 summarizes the number of acid sites of the studied compounds, expressed in millimoles of NH_3 per gram and millimoles of NH_3 per square meter. Acidity assessment with NH_3 as probe molecule is likely to overestimate the amount of LAS due to the formation of NH_3 clusters constituted of hydrogen-bonded molecules. Although all NH_3 that is not removed at 100 °C is commonly considered chemisorbed, in practice, it cannot be ruled out that part of the NH_3 remains adsorbed due to NH_3-NH_3 interactions. This presumption would explain the outstanding total surface acidity values observed for the synthesized porous hexacyanometallate(III) complexes.

Table 8. Acid properties of the studied hexacyanometallates(III).

Compound	Total Acidity [a] (μmol NH_3 g^{-1})	Acid Sites Density [a] (μmol NH_3 m^{-2})
Ni-Co	1880	5.0
Co-Co	2780	3.5
Fe-Co	2010	2.7
Ni-Fe	1960	12.2
Co-Fe	3780	6.1
Fe-Fe	1550	7.3

[a] Total amount of acid sites was determined assuming 1:1 stoichiometry for NH_3 adsorption on surface acid site.

When the density of LAS is measured per unit specific surface area, an inverse relationship is observed with the crystallite size of the samples (Figure 9). It should be noted that CUMSs can be generated by defects inside the cyanometallate crystal (bulk defects), but also by defects in the crystal boundary (surface defects). Therefore, it is reasonable to think that the smaller the crystallite size, the higher the surface-to-volume ratio, and consequently the higher the density of surface defects (i.e., CUMSs or LAS). This reasoning would also explain the increase in the T/M ratio measured by XRF when the crystallite size is reduced (see Table 5).

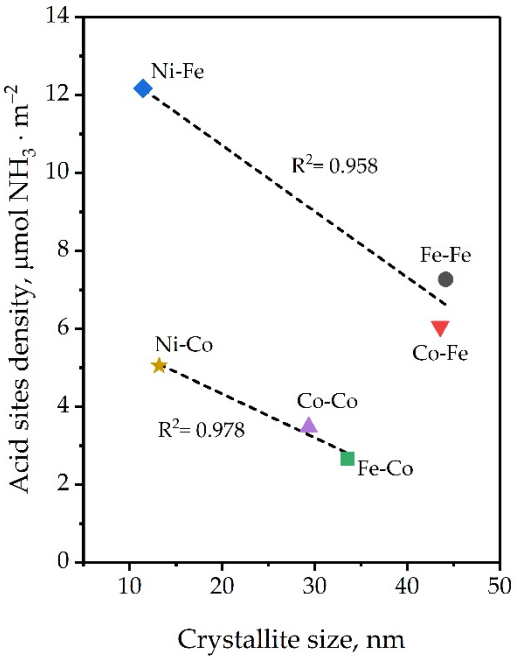

Figure 9. Relationship between acid site density and crystallize size in the studied porous hexacyanometallates(III).

Notwithstanding the foregoing, these results are likely to be misleading, because NH_3 penetrates where N_2 (kinetic diameter = 3.64 Å) cannot. Thus, the measured specific surface area is probably underestimated. Moreover, it is likely that the presence of a basic molecule such as NH_3 could prevent the structure distortion due to dehydration during heating. These considerations could explain why T-Fe compounds show higher acidity, in mmol NH_3 per m^2, than their T-Co counterparts.

2.2. Catalytic Activity Tests

The catalytic performance of the hexacyanometallate(III) complexes was evaluated in one-pot copolymerization of CO_2 and PO at 90 °C and 20 bar of CO_2 during 24 h. Previous to the reaction, all hexacyanometallates(III) were dehydrated in situ in vacuum conditions. Table 9 summarizes the results of the copolymerization reactions. Notably, all studied porous hexacyanometallate(III) compounds showed activity in the target reaction. To the best of our knowledge, this is the first time that any of these compounds has been reported as active catalytic material for the reaction under study. The key parameter controlling the activity seems to be S_{ext} (Pearson correlation coefficient = 0.950). Selectivity of both CO_2 and PO increased with T metal, in the order $Fe^{2+} < Co^{2+} < Ni^{2+}$, which agrees with the electronegativity of those metals. These results would indicate that the selectivity of CO_2/PO copolymerization could be controlled by the coordination ability of the LAS. The Fe-Fe complex constitutes an exception, since the T metal is Fe^{3+}, so its electronegativity is higher than its counterparts. However, its selectivity is lower. The reason could lie in the effect that the inner transition metal cation has on that selectivity.

Table 9. Catalytic performance of the studied porous hexacyanometallates(III) [a].

Compound	Yield [b] (g)	TOF [c]	F_{CU} [d] mol (%)	F_{CO2} [e] (wt%)	W_{PC} [f] (wt%)	S_{CO2} [g] (%)	S_{PO} [h] (%)	R_{PEC} (%)	M_w (g mol^{-1})	$Đ_M$
Ni-Co	3.2	4	22.3	14.4	0.4	98.9	99.7	79.5	11,800	10.5
Co-Co	18.9	23	20.0	13.1	4.2	87.4	97.2	71.9	68,600	4.1
Fe-Co	14.8	18	16.3	11.0	8.4	73.6	94.5	75.1	85,400	6.3
Ni-Fe	3.0	4	24.0	15.3	0.6	98.4	99.6	73.9	11,700	15.8
Co-Fe	11.6	12	33.5	20.2	13.3	75.4	90.2	66.0	50,000	5.9
Fe-Fe	6.0	7	17.3	11.6	43.1	26.2	67.2	83.3	6000	8.4

[a] All copolymerizations were carried out at 90 °C, 20 bar of CO_2, 104 mg of porous hexacyanometallate(III) with 50 mL of PO for 24 h. [b] Product was dried in vacuo at 40 °C during 24 h. [c] TOF is expressed in mol PO · (mol T)$^{-1}$ · h^{-1}. Mol of T was worked out from ideal catalyst formulation: $T_3[M(CN)_6]_2$. For Fe^{2+}-Fe^{3+}, formula was substituted by its real formula: $Fe_4[Fe(CN)_6]_3$. [d] Molar fraction of carbonate units (F_{CU}) determined by ^{1}H-NMR. [e] Mass fraction of CO_2 (F_{CO2}) determined by ^{1}H-NMR. [f] Weight percentage of cyclic propylene carbonate (W_{PC}) determined by ^{1}H-NMR. [g,h] CO_2 and PO selectivity determined by ^{1}H-NMR.

The chemical nature of the isolated products was analyzed via IR (Figure 10) and ^{1}H-NMR spectroscopy (Figure 11). Absorption peaks at 1745 and 1250 cm^{-1} are ascribed to the stretching vibration of the carbonyl bond (C=O) and the ether linkage (C-O-C) in the carbonate group, respectively. Their presence on the FT-IR spectra of the products indicates the successful incorporation of CO_2 into the polymer backbone. The peak at 1065 cm^{-1} indicates the formation of ether linkages as a result of consecutive PO enchainment. ^{1}H-NMR spectra confirm the existence of both carbonate and ether segments in the obtained polymers. The amount of CO_2 in the polymer varied between 11 and 20%, which indicates the strong tendency of the studied hexacyanometallates(III) toward PO homopolymerization. From this fact, polymers should be considered polyethercarbonates (PECs) rather than perfectly alternating polycarbonates. Production of cyclic PC was evidenced by proton peaks at 1.45–1.51 ppm and 4.45–4.50 ppm (see Figure 11). In the IR spectra, the presence of PC was evidenced by a peak at 1780 cm^{-1} corresponding to the ν(C=O) band. Broad absorption peaks around 3500 cm^{-1} in FT-IR spectra represent the stretching vibration of hydroxyl end groups. Their intensity is highly dependent on the molecular weight of the samples; that is to say, on the density of chain end groups. Such hydroxyl end groups could come from chain transfer reactions with protic impurities (water).

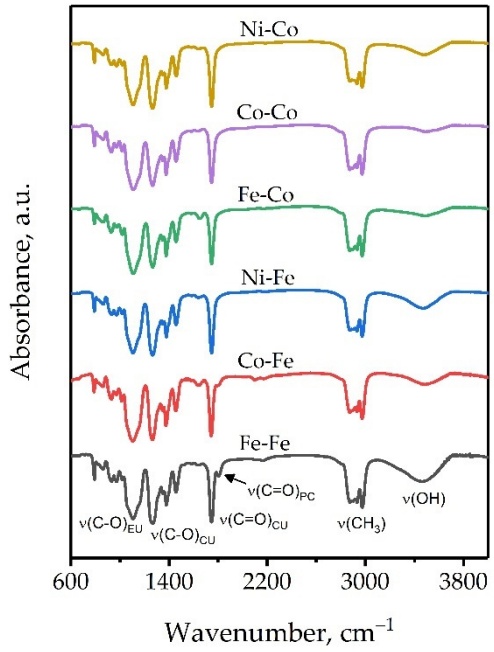

Figure 10. FT-IR spectra of products of CO_2/PO copolymerization.

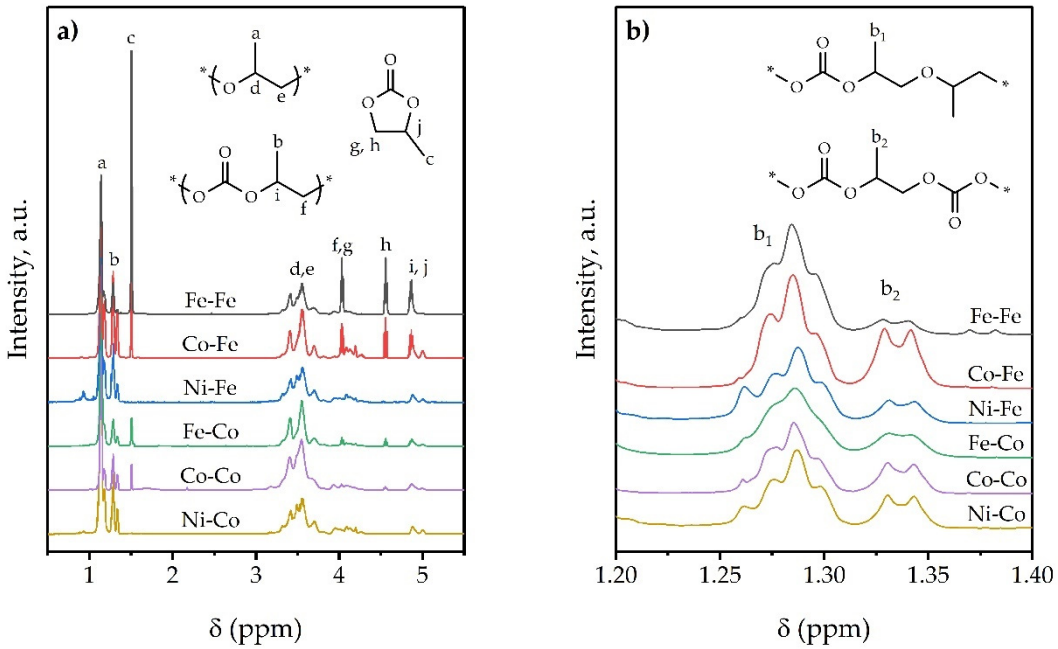

Figure 11. ^{1}H-NMR spectra of the obtained products (**a**) in the region from 0.5 to 5.5 ppm and (**b**) in the region corresponding to methyl entities of carbonate units (1.2–1.4 ppm). Peak assignment was made based on [91,92]. Detailed ^{1}H-NMR spectra of products are provided in Supplementary Materials (Figures S7–S12).

Additional information about the microstructure of the PECs can be obtained by dividing the methyl (CH_3, 1.25–1.38 ppm) signal of the carbonate units in two parts (see Figure 11b). The peak from 1.25–1.32 ppm (b_1) corresponds to a methyl group between a carbonate and an ether entity, whereas the peak from 1.32–1.38 ppm (b_2) corresponds to a methyl group between two adjacent carbonate units [92]. The polyethercarbonate/polycarbonate linkage ratio provides information about the pattern of configuration of the copolymers. While a random copolymer will possess a significant proportion of PEC linkages, a blocked copolymer will possess a lower density of PEC linkages. The obtained

copolymers showed a high proportion of PECs linkages (>70%), confirming their random structure.

Molecular weight and molecular weight distribution were analyzed by GPC (Figure S13). Average molecular weight (M_w) ranged between 6000 and 85,400 Da with broad dispersity ($Đ_M$) (5.9–15.8), characteristic of multiple-site-type heterogeneous polymerization catalysts. It is worth noting that no correlation was found between the density of surface LAS and molecular weight. On the one hand, many of the CUMSs titrated with NH_3 are inside the micropores, therefore they are not available for the copolymerization reaction. On the other hand, although every LAS represents an available coordination site for PO molecules, in order to proceed with the ring-opening of any coordinated PO, a nucleophilic attack is needed. The nucleophile species can be inherent to the catalysts or can be added as a co-catalyst. As we have been able to verify, hexacyanometallates(III) afford the ring-opening of PO without the need for a co-catalyst, so the nucleophile must come from the catalyst itself. Therefore, a true active site must be composed of both LAS and nucleophile species, which can be attached to the LAS itself (monometallic pathway) or to an adjacent LAS (bimetallic pathway). Considering that the distance between adjacent T metals is of the order of 10 Å, according to XRD, we propose that ring-opening occurs via a monometallic pathway. Finally, we must highlight the fact that although CAs are usually considered nucleophilic species [93,94], the hexacyanometallates(III) synthesized here did not show retention of CAs in their structure. Consequently, other species, such as Cl atoms, must act as the nucleophilic species.

Comparison of the Performance of the Studied Compounds with Other Cyanometallate Catalysts for CO_2/PO Copolymerization

According to the basis used by Coates and Moore to classify qualitatively the performance of catalytic systems for CO_2/epoxide copolymerization reaction, the activity studied porous hexacyanometallates(III) lies between moderate (turn-over frequency, TOF = 5–200 h^{-1}) and low values (TOF < 5 h^{-1}) [95]. These activity values are in the range of other heterogeneous catalysts used in this field, such as diethylzinc/active hydrogen-containing compound [96], zinc-dicarboxylates [97–99] or rare earth metal coordination catalysts [100–102]. However, comparison between the hexacyanometallate(III) complexes here studied and those catalysts is useless since the latter lead to perfectly, or almost perfectly, alternating polycarbonates. Cyanometallates, by contrast, tend to produce PECs with different CO_2 content as well as notable quantities of cyclic byproducts. Therefore, when comparing the performance of cyanometallate catalysts several parameters must be considered: TON, TOF, F_{CU}, W_{PC}, S_{CO2}, Mn and/or Mw and $Đ_M$. Table 10 presents comparison of the catalytic performance of the studied porous hexacyanometallates(III) with that of other cyanometallate compounds published.

Although direct comparison is difficult here because of the differences in reaction conditions and catalysts preparation, it can be concluded that productivity of the synthesized porous hexacyanometallates(III) is far lower than those of the well-known Zn-Co complex and the bidimensional Co-Ni compound, which are the cyanometallates that have been reported, up to now, to have better industrial prospects. Given the high tendency of cyanometallate catalysts to produce PECs with low CO_2 content, the molar fraction of carbonate units represents a key parameter when comparing different catalysts. The amount of CO_2 incorporated into polymer can be tuned by changing the CO_2 pressure and the reaction temperature. The studied porous hexacyanometallates(III) have given rise to polymers with slightly higher F_{CU} values than their counterparts, even though we carried out the reaction at relatively lower CO_2 pressures. Only the Zn-Ni compound, along with the bidimensional complexes tested by Robertson et al. [56] show higher CO_2 uptake. These results demonstrate that the selection of outer transition metal cations other than Zn^{2+} can be a good solution in order to achieve cyanometallate catalysts with higher CO_2 incorporation capacity. In terms of selectivity, the studied complexes show values similar to those reported in Zn^{2+}-based complexes. The bidimensional Co-Ni, Co-Pd and Co-Pt complexes do not produce cyclic PC. Molecular weight achieved with the studied

compounds are between those produced by the Zn^{2+}-based cyanometallates and the bidimensional complexes. However, comparison is particularly difficult here because some of the reported compounds were tested in the presence of a chain transfer agent which reduced the molecular weight of the final product.

Table 10. Comparison of the performance of the studied porous hexacyanometallate(III) complexes with other cyanometallate catalysts in the copolymerization of CO_2 and PO.

Catalyst Formulation	Time (h)	PO/Cat. (g/g)	P (bar)	T (°C)	TON [a]	TOF [b]	F_{CU} (mol%)	W_{PC} (wt%)	S_{CO2} (%)	Mw (g mol^{-1})	$Đ_M$	Ref
$Ni_3[Co(CN)_6]_2$	24	400	20	90	86	4	22	0.4	99	11,800	10.5	-
$Co_3[Co(CN)_6]_2$	24	400	20	90	544	23	20	4.2	87	68,600	4.1	-
$Fe_3[Co(CN)_6]_2$	24	400	20	90	428	18	16	8.4	74	85,400	6.3	-
$Ni_3[Fe(CN)_6]_2$	24	400	20	90	84	4	15	0.6	98	11,700	15.8	-
$Co_3[Fe(CN)_6]_2$	24	400	20	90	296	12	20	13.3	75	50,000	5.9	-
$Fe_4[Fe(CN)_6]_3$	24	400	20	90	162	7	17	43.1	26	6000	8.4	-
$Zn_3[Co(CN)_6]_2$	10	42,000	38	90	64,414	6441	13	4.4	82	10,800	1.8	[103]
$Zn_3[Fe(CN)_6]_2$ [c]	10	4611	50	110	137	14	15	62.5	12	2160	n.a.	[50]
$Zn_3[Cr(CN)_6]_2$ [c]	10	4611	50	140	334	33	10	36.6	22	1350	n.a.	[50]
$Zn[Cd(CN)_4]$ [c]	10	4611	50	130	35	4	2	6.5	33	n.a.	n.a.	[50]
$Zn_2[Mo(CN)_8]$ [c]	10	4611	50	130	196	20	14	16.5	53	1420	n.a.	[50]
$Zn_2[Fe(CN)_6]_2$ [c]	10	4611	50	110	233	23	5	77.8	2	n.a.	n.a.	[50]
$Zn[Ni(CN)_4]$	20	553	50	110	210	11	62	6.6	91	2360	1.8	[91]
$Co[Ni(CN)_4]_2$	1	664	54.4	90	1510	1510	27	-	100	526,400	2.8	[56]
$Co[Pd(CN)_4]_2$	1	546	54.4	90	18	18	43	-	100	92,160	3.6	[56]
$Co[Pt(CN)_4]_2$	1	411	54.4	90	13	13	44	-	100	103,230	3.7	[56]

[a] TON is expressed in mol PO · (mol T)$^{-1}$. [b] TOF is expressed in mol PO · (mol T)$^{-1}$ · h^{-1}. [c] Catalyst was tested in the presence of chain transfer agents.

3. Materials and Methods

3.1. Materials

Cyanometallate precursor salts ($K_3Co(CN)_6$ and $K_3Fe(CN)_6$), along with divalent transition metal cation precursor salts ($CoCl_2$, $FeCl_2$ and $NiCl_2$, all with 98% purity), were purchased from Sigma-Aldrich and used as received. *Tert*-butyl alcohol (TBA, 99.5%) and propylene oxide (PO, 99.5%) were provided by ACROS Organics and used without extra purification. CO_2 with a purity of 99.99% (Air Liquide) was used as supplied.

3.2. Preparation of Porous Hexacyanometallates(III)

Divalent transition metal hexacyanometallates(III) were prepared by a coprecipitation method adapted from the classic procedure reported elsewhere for cyanometallate catalysts [91,104–106]. TBA was used as organic CA and TCl_2 salts were fed in an excess of 300% with respect to stoichiometric requirements. This excess percentage corresponds to a value of 6 for the T/M initial preparation ratio. More details are given below.

$K_3[M(CN)_6]$ (0.16 M) aqueous solution was added at a rate of 5 mL min^{-1} to TCl_2 (1.6 M) aqueous solution containing TBA (TBA/water = 1:3 *v/v*). The resulting suspension was kept under vigorous stirring at 30 °C for 20 min and then centrifugated at 4200 rpm for 30 min. The slurry obtained was resuspended in a mixture of TBA/water (1:1, *v/v*) and aged for 20 min at 30 °C while stirring. The solid was separated again by centrifugation under the same conditions as previously. This process was repeated one more time, increasing the ratio TBA/water to 3:1 (*v/v*). Finally, the wet catalyst formed was suspended in pure TBA, kept for 20 min at 30 °C, centrifuged, and dried under low pressure at 50 °C until constant weight.

3.3. CO_2/PO Copolymerization Procedure

CO_2/PO copolymerization was performed in a 300 mL Hastelloy C-276 reactor equipped with a MagneDrive® II magnetic stirrer, pressure indicator, cooling coil, and clamp band heater. The reactor was charged with the calculated amount of catalyst and purged with 100 mL min^{-1} of N_2 for 30 min. Then the catalyst was dehydrated in situ under vacuum conditions for 1 h. The dehydration temperature of each complex was determined by thermogravimetric analysis (TGA). After that, the reactor was cooled down and PO was fed at room temperature at reduced pressure. Afterwards, the reactor was pressurized with 10 bar of CO_2, to maintain the PO in the liquid state, and heated to the operation temperature. Once the reaction temperature was reached, more CO_2 was fed until 20 bar. Pressure was kept constant throughout the reaction by feeding fresh CO_2 as the pressure inside the reactor decreased. Copolymerization was stopped after 24 h. The resulting, colored product was dissolved in chloroform and filtered to remove residual catalyst and dried at 40 °C in vacuum for 24 h. The final product thus obtained was totally transparent.

3.4. Characterization

3.4.1. Porous Hexacyanometallate(III) Characterization

X-ray diffraction (XRD) patterns were recorded on a Philips X'pert PRO using Cu-K_α (λ = 1.541874 Å). Data were collected from 5 to 50° 2θ with a step size and step time of 0.026° and 598 s, respectively.

Fourier-transform infrared spectroscopy (FT-IR) spectra were obtained with a FT-IR spectrometer (Jasco 4200) at 4 scans per spectrum at a resolution of 4 cm^{-1}. Samples were processed using the KBr pressed disk technique (2 mg of sample and 178 mg of KBr).

TGA was used to evaluate the thermal behavior and degree of hydration of the studied compounds. TGA was carried out on a SETSYS Evolution device (Setaram) in oxidizing (air) and inert (N_2) atmosphere with temperature ramped from 25 to 950 °C at a rate of 1 °C min^{-1}. To discriminate between the weight loss stages corresponding to water, TBA, and decomposition, evolved gas analysis (EGA) was carried out, coupling the TGA with a QMG-220 Prisma Plus compact mass spectrometer (MS; Pfeiffer Vacuum).

In situ high-temperature X-ray diffraction (HTXRD) studies were carried out to shed light on the thermal stability and dehydration process of divalent transition metal hexacyanometallates(III). XRD data were collected on a Bruker D8 Advance diffractometer operating at 30 kV and 20 mA, equipped with a Cu tube (λ = 1.5418 Å), a Vanted-1 PSD detector, and an Anton Parr HTK2000 high-temperature furnace. The powder patterns were recorded in 2θ steps of 0.033° in the $10° \leq 2\theta \leq 70°$ range, counting for 0.8 s per step (total time for each temperature = 26 min). Datasets were recorded from 30 to 250 °C every 10 °C at a heating rate of 1 °C min^{-1}.

Elemental analysis (EA) was conducted with a Euro EA 3000 Elemental Analyzer (CHNS, EuroVector). The instrument was calibrated for CHN with acetanilide standard. Samples were burned at 980 °C in a He stream enriched with high-purity O_2. The resulting components, N_2, CO_2, and H_2O, were separated in a chromatographic column and detected by a thermo conductivity detector. Peak analysis was performed by Callidus® software.

X-ray fluorescence (XRF) was used to measure the weight percentage of inorganic elements in the catalysts. The samples were analyzed in powder form in a PANalytical/AXIOS wavelength dispersive spectrometer (WDXRF). Since no calibration curves were available, the analysis was semi-quantitative. The obtained values were adjusted based on the organic content (C, H, N, O) collected from EA and TGA techniques.

The morphology and size of catalyst particles were evaluated in detail by scanning electron microscopy (SEM) and transmission electron microscopy (TEM). SEM images were taken by a Hitachi S-4800 operating at 10 kV, and TEM pictures were obtained from a JEM-1400 Plus instrument using a voltage of 100 kV.

The textural properties of the catalysts were determined by physisorption of N_2 at 77 K. Isotherms were collected in a Micromeritics ASAP 2020 (accelerated surface area and

porosity system). Prior to the analysis, all samples were evacuated at 150 °C for 10 h to remove any water and TBA that may have been in the pores.

The number of CUMSs was assessed by ammonia (NH_3) adsorption under flowing dynamic experiments. The amount of NH_3 chemisorbed on the catalysts was determined gravimetrically by using TGA. The hexacyanometallate(III) samples, typically 40–50 mg, were suspended in the pan of the microbalance and pretreated with 50 mL min^{-1} of He at 150 °C for 3 h. Afterwards, samples were cooled down to 100 °C and exposed to a dilute stream of NH_3 in He for 1 h. Then, samples were evacuated for 2 h at 100 °C in He (50 mL min^{-1}) in order to leave out physisorbed NH_3.

3.4.2. Polymer Characterization

The structure of the copolymers was studied via infrared analysis in a Jasco 4200 device with 40 scans per experiment at a resolution of 1 cm^{-1}. KBr disks were prepared by casting an acetone solution of the polymers onto them.

Proton nuclear magnetic resonance (^{1}H-NMR) spectra were collected at 500 MHz on a Bruker AV-500 spectrometer employing $CDCl_3$ as solvent. Chemical shifts were referenced with respect to residual solvent ($CDCl_3$) signal. Integration of ^{1}H-NMR signals was used to determine the molar fraction of carbonate units (F_{CU}) in the polymer chain and the weight percentage of cyclic propylene carbonate (PC) (W_{PC}) following Equations (1) and (2) [91]:

$$F_{CU},\ \text{mol\%} = \frac{A_{5.0} + A_{4.13} - 2A_{4.48}}{(A_{5.0} + A_{4.13} - 2A_{4.48}) + A_{3.5}} \times 100 \quad (1)$$

$$W_{FC},\ \text{wt.\%} = \frac{102A_{1.48}}{58A_{1.14} + 102\ (A_{1.3} + A_{1.48})} \times 100 \quad (2)$$

where A_x represents the area under the corresponding ^{1}H-NMR peak. The mass fraction of CO_2 (F_{CO2}) in the polymer was calculated by adapting Equation (1) to Equation (3):

$$F_{CO_2},\ \text{wt.\%} = \frac{44\ (A_{5.0} + A_{4.13} - 2A_{4.48})}{102\ (A_{5.0} + A_{4.13} - 2A_{4.48}) + 58A_{3.5}} \times 100 \quad (3)$$

The selectivity of CO_2 (S_{CO2}) and PO (S_{PO}) toward polymers in detriment of PC was calculated using Equations (4) and (5):

$$S_{CO_2},\ \% = \frac{A_{1.3}}{A_{1.3} + A_{1.48}} \times 100 \quad (4)$$

$$S_{PO},\ \% = \frac{A_{1.14} + A_{1.3}}{A_{1.14} + A_{1.3} + A_{1.48}} \times 100 \quad (5)$$

The polyethercarbonate/polycarbonate linkage ratio (R_{PEC}) was determined through Equation (4):

$$R_{PEC}, \% = \frac{A_{1.29}}{A_{1.29} + A_{1.35}} \times 100 \quad (6)$$

Gel permeation chromatography (GPC) data were collected using a Waters 717plus Autosampler and a Waters 515 HPLC pump connected to a Waters 2414 refractive index detector equipped with Waters Styragel HR-1 and HR-4 columns using THF as eluent. The flow rate, column temperature, and injection volume were set to 1 mL min^{-1}, 40 °C, and 70 μL, respectively. Columns were calibrated with narrow Mw polystyrene standards.

4. Conclusions

Although divalent transition metal hexacyanometallates(III) have received a great deal of attention in the last few years due to their outstanding properties and suitability for dozens of applications, their catalytic capabilities still remain unknown for most of the scientific community. In this contribution, a set of well-ordered porous divalent transition metal hexacyanometallate(III) complexes was synthesized by a TBA-assisted

coprecipitation method. The bimetallic character of the synthesized compounds was confirmed by IR spectroscopy. The chemical formula of the compounds corresponded to the expected $T_3[Co(CN)6]_2 \cdot xH_2O$, except the Fe-Fe compound, which suffered chemical changes during the synthesis procedure, resulting in the well-known Prussian blue complex: $Fe_4[Fe(CN)6]_3 \cdot xH_2O$. According to the XRD patterns, all complexes were isostructural, crystallizing in a cubic fm-3m lattice. Pore width and crystallite size were modulated by the electronegativity of outer and inner transition metal cations. The synthesized hexacyanometallates(III) were shown to be extremely sensitive to temperature. All of them decomposed at temperatures above 300 °C, and partial decomposition was observed in the Fe-Co, Ni-Fe, and Fe-Fe samples at temperatures as low as 150 °C. The dehydration process involves reversible distortion and contraction of the porous framework, which shows the structural flexibility of these compounds. TBA was shown to act as a capping agent during synthesis, giving rise to tiny nanocrystals that agglomerated to form a network of micro-mesopores. The size of the grains was again highly dependent on the electronegativity of the transition metals involved. N_2 accessibility to the micropores was affected by structural shrinkage due to dehydration during pretreatment. The Fe-Fe, Ni-Fe, and Fe-Fe samples were especially affected by the pretreatment. Acidity assessment employing NH_3 as probe molecule led to outstanding acidity values. The density of acid sites per unit specific surface area was determined by the crystallite size of the samples, likely because of an increase in surface defects with increased surface-to-volume ratio.

Porous hexacyanometallates(III) were screened in batch copolymerization of PO and CO_2 at a moderate temperature (90 °C) and 20 bar over 24 h. All studied complexes were active in the given reaction. They yielded aliphatic polyethercarbonates characterized by modest CO_2 content and moderate molecular weight (M_w = 6000–85,400 g/mol) with a broad distribution ($Đ_M$ = 4.1–15.8). Catalytic activity was highly affected by the external surface. The generation of cyclic PC as a byproduct was registered in a large percentage range (0.4–43.1%). Selectivity was determined by the electronegativity of the transition metal cations, especially the outer one. A closer look at the ^{1}H-NMR spectra allowed us to identify the random configuration of polyethercarbonate copolymers.

Supplementary Materials: The following are available online at https://www.mdpi.com/article/10.3390/catal11121450/s1, Figure S1: Williamson–Hall plot of studied complexes; Figure S2: Relationship between unit cell edge length and ν(CN) band in cyanocobaltates; Figure S3: Evolution of XRD peaks with temperature; Figure S4: Relationship between T/M atomic ratio and crystallite size in studied compounds; Figure S5: PSD of studied compounds; Figure S6: NH_3-saturation curves of studied compounds; Figure S7: SEC plots of polyethercarbonates obtained; Figure S8: Detailed 1H-NMR spectrum for the product obtained employing the Co-Co complex; Figure S9: Detailed 1H-NMR spectrum for the product obtained employing the Fe-Co complex; Figure S10: Detailed 1H-NMR spectrum for the product obtained employing the Ni-Fe complex; Figure S11: Detailed 1H-NMR spectrum for the product obtained employing the Co-Fe complex; Figure S12: Detailed 1H-NMR spectrum for the product obtained employing the Fe-Fe complex; Figure S13: SEC plots (log Mw) of the polyethercarbonates (PECs) formed using the studied porous hexacyanometallates(III); Table S1: Dubinin–Asthakov parameters for studied compounds.

Author Contributions: G.P. conceived, designed, and performed the experiments, analyzed the data, and prepared the original draft. M.P.G.-M. supervised the research, formally analyzed the experiments and data, and revised and corrected the manuscript. J.R.G.-V. conceptualized and supervised the research, revised the final manuscript, and acquired the funding. All authors have read and agreed to the published version of the manuscript.

Funding: This research was funded by the Spanish Ministry of Science and Innovation (Project PID2019-105960RBC21) and the Basque Government (GIC-IT1297-19). One of the authors (G.P.) is the recipient of a PhD research fellowship provided by the Basque Government (PRE_2021_2_0260).

Data Availability Statement: The data presented in this study are available in the article or the Supplementary Materials.

Acknowledgments: The authors thank the technical and human support provided by SGIker.

Conflicts of Interest: The authors declare no conflict of interest.

References

1. Piernas-Muñoz, M.J.; Castillo-Martínez, E. *Prussian Blue-Based Batteries*; Springer: Cham, Switzerland, 2018.
2. Wojdel, J.C.; Bromley, S.T.; Illas, F.; Jansen, J.C. Development of realistic models for Double Metal Cyanide catalyst active sites. *J. Mol. Model.* **2007**, *13*, 751–756. [CrossRef]
3. Imanishi, N.; Morikawa, T.; Kondo, J.; Yamane, R.; Takeda, Y.; Yamamoto, O.; Sakaebe, H.; Tabuchi, M. Lithoum intercalation behavior of iron cyanometallates. *J. Power Source* **1999**, *81*, 530–534. [CrossRef]
4. Hanusa, T.P. Cyanide complexes of the transition metals. In *Encyclopedia of Inorganic Chemistry and Bioinorganic Chemistry*, 1st ed.; King, R.B., Ed.; John Wiley & Sons: Hoboken, NJ, USA, 2006.
5. Hibble, S.J.; Cheyne, S.M.; Hannon, A.C.; Eversfield, S.G. CuCN: A polymorphic material. Structure of one form determine from total neutron diffraction. *Inorg. Chem.* **2002**, *41*, 4990–4992. [CrossRef] [PubMed]
6. Hibble, S.J.; Wood, G.B.; Bilbé, E.J.; Pohl, A.H.; Tucker, M.G.; Hannon, A.C.; Chippindale, A.M. Structures and negative thermal expansion properties of the one-dimensional cyanides, CuCN, AgCN and AuCN. *Z. Kristallogr.* **2010**, *225*, 457–462. [CrossRef]
7. Hibble, S.J.; Cheyne, S.M.; Hannon, A.C.; Eversfield, S.G. Beyond bragg scattering: The structure of AgCN determined from total neutron diffraction. *Inorg. Chem.* **2002**, *41*, 1042–1044. [CrossRef]
8. Zhang, K.; Lee, T.H.; Bubach, B.; Ostadhassan, M.; Jang, H.W.; Choi, J.; Shokouhimehr, M. Layered metal-organic framework based on tetracyanonickelate as a cathode material for in situ Li-ion storage. *RSC Adv.* **2019**, *9*, 21363–21370. [CrossRef]
9. Kitazawa, T.; Fukunaga, M.; Takahashi, M.; Takeda, M. Study by X-ray crystallography and Mössbauer spectroscopy of the layered compounds with two-dimensional metal complex iron(II) tetracyanonicketale(II). *Mol. Cryst. Liq. Cryst.* **1994**, *244*, 331–336. [CrossRef]
10. Hibble, S.J.; Chippindale, A.M.; Bilbé, E.J.; Marelli, E.; Harris, P.J.F.; Hannon, A.C. Structures of $Pd(CN)_2$ and $Pt(CN)_2$: Intrinsically nanocrystalline materials? *Inorg. Chem.* **2011**, *50*, 104–113. [CrossRef]
11. Weiser, H.B.; Milligan, W.O.; Bates, J.B. X-Ray diffraction studies on heavy-metal iron-cyanides. *J. Phys. Chem.* **1942**, *46*, 99–111. [CrossRef]
12. Grandjean, F.; Samain, L.; Long, G.J. Characterization and utilization of Prussian blue and its pigments. *Dalton Trans.* **2016**, *45*, 18018–18044. [CrossRef]
13. Müller, H.; Müller, W.; Wehner, M.; Liewald, H. Artists' colors. In *Ullman's Encyclopedia of Industrial Chemistry*; Wiley-VCH: Weinheim, Germany, 2012; Volume 4, pp. 241–254.
14. Sato, O.; Iyoda, T.; Fujishima, A.; Hashimoto, K. Photoinduced magnetization of cobalt-iron cyanide. *Science* **1996**, *272*, 704–705. [CrossRef]
15. Fornasieri, G.; Bordage, A.; Bleuzen, A. Magnetism and photomagnetism of Prussian blue analogue nanoparticles. *Eur. J. Inorg. Chem.* **2018**, 259–271. Available online: https://chemistry-europe.onlinelibrary.wiley.com/doi/full/10.1002/ejic.201700819 (accessed on 24 November 2021). [CrossRef]
16. Yuan-Fu, X.; Zhi, Y.; Yong, S.; Hong-Bo, H.; Xiao-Zeng, Y.; Zhou, X.Z.; Li, Z.W.; Kunkel, H.P.; Williams, G. Mössbauer evidence for ferromagnetic ordering in copper-iron cyanometallates. *Chin. Phys. Lett.* **2002**, *19*, 595–598. [CrossRef]
17. Ferlay, S.; Mallah, T.; Ouahès, R.; Veillet, P.; Verdaguer, M. A room-temperature organometallic magnet based on Prussian blue. *Nature* **1995**, *378*, 701–703. [CrossRef]
18. Rogez, G.; Marvilliers, A.; Sarr, P.; Parsons, S.; Teat, S.J.; Ricard, L.; Mallah, T. Tuning the optical properties of Prussian blue-like complexes. *Chem. Commun.* **2002**, *14*, 1460–1461. [CrossRef] [PubMed]
19. Jain, A.K.; Singh, R.P.; Bala, C. Solid membranes for copper hexacyanoferrate(II) as thallium(I) sensitive electrode. *Anal. Lett.* **1982**, *15*, 1557–1563. [CrossRef]
20. Tani, Y.; Eun, H.; Umezawa, Y. A cation selective electrode based on copper(II) and nickel(II) hexacyanoferrates: Dual response mechanism, selective uptake or adsorption of analyte cations. *Electrochim. Acta* **1998**, *43*, 3431–3441. [CrossRef]
21. Li, W.; Han, C.; Cheng, G.; Chou, S.; Liu, H.; Dou, S. Chemical properties, structural properties, and energy storage applications of Prussian blue analogues. *Small* **2019**, *15*, 1900470. [CrossRef]
22. Hurlbutt, K.; Wheeler, S.; Capone, I.; Pasta, M. Prussian blue analogs as battery materials. *Joule* **2018**, *2*, 1950–1960. [CrossRef]
23. Kaye, S.S.; Long, J.R. The role of vacancies in the hydrogen storage properties of Prussian blue analogues. *Catal. Today* **2007**, *120*, 311–316. [CrossRef]
24. Reguera, L.; Balmaseda, J.; Krap, C.P.; Reguera, E. Hydrogen storage in porous transition metal nitroprussides. *J. Phys. Chem. C* **2008**, *112*, 10490–10501. [CrossRef]
25. Zamora, B.; Roque, J.; Balmaseda, J.; Reguera, E. Methane storage in Prussian blue analogues and related porous solids: Nature of the involver adsorption forces. *Z. Anorg. Allg. Chem.* **2010**, *636*, 2574–2578. [CrossRef]
26. Chapman, K.W.; Southon, P.D.; Weeks, C.L.; Kepert, C.J. Reversible hydrogen gas uptake in nanoporous Prussian blue analogues. *Chem. Commun.* **2005**, *26*, 3322–3324. [CrossRef]
27. Barton, G.B.; Hepworth, J.L.; McClanahan, E.D.; Moore, R.L.; Van Tuyl, H.H. Chemical processing wastes: Recovering fission products. *Ind. Eng. Chem.* **1958**, *50*, 212–216. [CrossRef]
28. Valvekens, P.; De Vos, D. Double metal cyanides as heterogeneous catalysts for organic reactions. In *New Materials for Catalytic Applications*; Parvulescu, V.I., Kemnitz, E., Eds.; Elvesier: San Diego, CA, USA, 2016; pp. 1–12.

29. Satyarthi, J.K.; Srinivas, D.; Ratnasamy, P. Influence of surface hydrophobicity on the esterification of fatty acids over solid catalysts. *Energy Fuels* **2010**, *24*, 2154–2161. [CrossRef]
30. Srinivas, D.; Satyarthi, J.K. Biodiesel production from vegetable oils and animal fat over solid acid double-metal cyanide catalysts. *Catal. Surv. Asia* **2011**, *15*, 145–160. [CrossRef]
31. Srivastava, R.; Srinivas, D.; Ratnasamy, P. Fe-Zn double-metal cyanide complexes as novel, solid transesterification catalysts. *J. Catal.* **2006**, *241*, 34–44. [CrossRef]
32. Yan, F.; Yuan, Z.; Lu, P.; Luo, W.; Yang, L.; Deng, L. Fe-Zn double-metal cyanide complexes catalyzed biodiesel production from high-acid-value oil. *Renew. Energy* **2011**, *36*, 2026–2031. [CrossRef]
33. Peeters, A.; Valvekens, P.; Vermoortele, F.; Ameloot, R.; Kirschhock, C.; De Vos, D. Lewis acid double metal cyanide catalysts for hydroamination of phenylacetylene. *Chem. Commun.* **2011**, *47*, 4114–4116. [CrossRef]
34. Patil, M.V.; Yadav, M.K.; Jasra, R.V. Prins condensation for synthesis of nopol from β-pinene and paraformaldehyde on novel Fe-Zn double metal cyanide solid acid catalyst. *J. Mol. Catal. A Chem.* **2007**, *273*, 39–47. [CrossRef]
35. García-Ortiz, A.; Grirrane, A.; Reguera, E.; García, H. Mixed (Fe^{2+} and Cu^{2+}) double metal hexacyanocobaltates as solid catalyst for the aerobic oxidation of oximes to carbonyl compounds. *J. Catal.* **2014**, *311*, 386–392. [CrossRef]
36. Belner, R.J. Method of Making a Polyether Using a Double Metal Cyanide Complex Compound. U.S. Patent 3,278,458A, 11 October 1996.
37. Herold, R.J.; Livigni, R.A. Hexacyanometalate salt complexes as catalysts for epoxide polymerization. In *Polymerization Kinetics and Technology*; Platzer, N.A.J., Ed.; American Chemical Society: Washington, DC, USA, 1973; pp. 208–229.
38. Kruper, W.J.; Swart, D.J. Carbon Dioxide Oxirane Copolymers Prepared Using Double Metal Cyanide Complexes. U.S. Patent 4,500,704A, 19 February 1985.
39. Dharman, M.M.; Yu, J.; Ahn, J.; Park, D. Selective production of cyclic carbonate over polycarbonate using a double metal cyanide-quaternary ammonium salt catalyst system. *Green Chem.* **2009**, *11*, 1754–1757. [CrossRef]
40. Saikia, L.; Satyarthi, J.K.; Gonnade, R.; Srinivas, D.; Ratnasamy, P. Double metal cyanides as efficient solid acid catalysts for synthesis of β-amino alcohols under solvent-free conditions. *Catal. Lett.* **2008**, *123*, 24–31. [CrossRef]
41. Peeters, A.; Valvekens, P.; Ameloot, R.; Sankar, G.; Kirschhock, C.E.A.; De Vos, D.E. Zn-Co double metal cyanides as heterogeneous catalysts for hydroamination: A structure-activity relationship. *ACS Catal.* **2013**, *3*, 597–607. [CrossRef]
42. Zhang, X.; Hua, Z.; Chen, S.; Liu, F.; Sun, X.; Qi, G. Role of zinc chloride and complexing agents in highly active double metal cyanide catalysts for ring-opening polymerization of propylene oxide. *Appl. Catal. A* **2007**, *325*, 91–98. [CrossRef]
43. Lee, I.K.; Ha, J.Y.; Cao, C.; Park, D.; Ha, C.; Kim, I. Effect of complexing agents of double metal cyanide catalyst on the copolymerization of cyclohexene oxide and carbon dioxide. *Catal. Today* **2009**, *148*, 389–397. [CrossRef]
44. Fernández-Dacosta, C.; Van der Spek, M.; Hung, C.R.; Oregionni, G.D.; Skagestad, R.; Parihar, P.; Gokak, D.T.; Strømman, A.H.; Ramirez, A. Prospective techno-economic and environmental assessment of carbon capture at a refinery and CO_2 utilisation in polyol synthesis. *J. CO2 Util.* **2017**, *21*, 405–422. [CrossRef]
45. Zhu, Y.; Romain, C.; Williams, C.K. Sustainable polymers from renewable resources. *Nature* **2016**, *540*, 354–364. [CrossRef]
46. Von der Assen, N.; Bardow, A. Life cycle assessment of polyols for polyurethane production using CO_2 as feedstock: Insight from an industrial case study. *Green Chem.* **2014**, *16*, 3272–3280. [CrossRef]
47. Zhang, W.; Lu, L.; Cheng, Y.; Xu, N.; Pan, L.; Lin, Q.; Wang, Y. Clean and rapid synthesis of double metal cyanide complexes using mechanochemistry. *Green Chem.* **2011**, *12*, 2701–2703. [CrossRef]
48. Dai, C.; Zhu, Q.; Pang, H.; Zhu, L.; Lin, Q. Rapid copolymerization of carbon dioxide and propylene oxide catalyzed by double metal cyanide complexes in an ultrasonic field. *Mater. Lett.* **2016**, *180*, 89–92. [CrossRef]
49. Guo, Z.; Lin, Q. Coupling reaction of CO_2 and propylene oxide catalyzed by DMC with co-complexing agents incorporated via ball milling. *J. Mol. Catal. A Chem.* **2014**, *390*, 63–68. [CrossRef]
50. Zhang, X.H.; Chen, S.; Wu, X.M.; Sun, X.K.; Liu, F.; Qi, G.R. Highly active double metal cyanide complexes. Effect of central metal and ligand on reaction of epoxide/CO_2. *Chin. Chem. Lett.* **2007**, *18*, 887–890. [CrossRef]
51. Qiang, L.; Zhifang, G.; Lisha, P.; Xue, X. Zn-Cr double metal cyanide catalysts synthesized by ball milling for the copolymerization of CO_2/propylene oxide, phtalic anhydride/propylene oxide, and CO_2/propylene oxide/phtalic anhydride. *Catal. Commun.* **2015**, *64*, 114–118. [CrossRef]
52. Chen, S.; Hua, Z.; Fang, Z.; Qi, G. Copolymerization of carbon dioxide and propylene oxide with highly effective hexacyanocobaltate(III)-based coordination catalyst. *Polymer* **2004**, *45*, 6519–6524. [CrossRef]
53. Qin, Y.; Wang, X. Carbon dioxide-based copolymers: Environmental benefits of PPC, and industrially viable catalyst. *Biotechnol. J.* **2010**, *5*, 1164–1180. [CrossRef] [PubMed]
54. Kember, M.R.; Buchard, A.; Williams, C.K. Catalysts for CO_2/epoxide copolymerization. *Chem. Commun.* **2011**, *47*, 141–163. [CrossRef] [PubMed]
55. Gao, Y.; Qin, Y.; Zhao, X.; Wang, F.; Wang, X. Selective synthesis of oligo(carbonate-ether) diols from copolymerization of CO2 and propylene oxide under zinc-cobalt double metal cyanide complex. *J. Polym. Res.* **2012**, *19*, 9878–9887. [CrossRef]
56. Robertson, N.J.; Qin, Z.; Dallinger, G.C.; Lobkovsky, E.B.; Lee, S.; Coates, G.W. Two-dimensional double metal cyanide complexes: Highly active catalysts for the homopolymerization of propylene oxide and copolymerization of propylene oxide and carbon dioxide. *Dalton Trans.* **2006**, *45*, 5390–5395. [CrossRef]

57. Alferov, K.; Wang, S.; Li, T.; Xiao, M.; Guan, S.; Meng, Y. Co-Ni cyanide bi-metal catalysts: Copolymerization of carbon dioxide with propylene oxide and chain transfer agents. *Catalysts* **2019**, *9*, 632. [CrossRef]
58. Ogilvie, S.H.; Duyker, S.G.; Southon, P.D.; Peterson, V.K.; Kepert, C.J. Identification of bridged CO_2 binding in a Prussian blue analogue using neutron powder diffraction. *Chem. Commun.* **2013**, *49*, 9404–9406. [CrossRef]
59. Ludi, A.; Güedel, H.U.; Rüegg, M. The structural chemistry of Prussian blue analogs. A single-crystal study of manganese(II) hexacyanocobaltate(III), $Mn_3[Co(CN)_6]_2 \cdot xH_2O$. *Inorg. Chem.* **1970**, *9*, 2224–22278. [CrossRef]
60. Kuyper, J.; Boxhoorn, G. Hexacyanometallate salts used as alkene-oxide polymerization catalysts and molecular sieves. *J. Catal.* **1987**, *105*, 163–174. [CrossRef]
61. Kaye, S.S.; Long, J.R. Hydrogen storage in the dehydrated Prussian blue analogues $M_3[Co(CN)_6]_2$ (M = Mn, Fe, Co, Ni, Cu, Zn). *J. Am. Chem. Soc.* **2005**, *127*, 6506–6507. [CrossRef]
62. Autie-Castro, G.; Autie, M.; Reguera, E.; Santamaría-González, J.; Moreno-Tost, R.; Rodríguez-Castellón, E.; Jiménez-López, A. Adsorption and separation of light alkane hydrocarbons by porous hexacyanocobaltates(III). *Surf. Interface Anal.* **2009**, *41*, 730–734. [CrossRef]
63. Nakamoto, K. *Infrared and Raman Spectra of Inorganic and Coordination Compounds*, 6th ed.; John Wiley & Sons: Hoboken, NJ, USA, 2009. [CrossRef]
64. Dunbar, K.R.; Heintz, R.A. Chemistry of transition metal cyanide compounds: Modern perspectives. In *Progress in Inorganic Chemistry*; Karlin, K.D., Ed.; John Wiley & Sons: Hoboken, NJ, USA, 1997; Volume 45, pp. 283–391. [CrossRef]
65. Ghosh, S.N. Infrared spectra of the Prussian blue analogs. *J. Inorg. Nucl. Chem.* **1974**, *36*, 2465–2466. [CrossRef]
66. Nakagawa, I.; Shimanouchi, T. Far infra-red spectra of some hexacyano-complex salts. *Spectrochim. Acta A Mol. Spectrosc.* **1970**, *26*, 131–141. [CrossRef]
67. Shriver, D.F.; Sheriver, S.A.; Anderson, S.E. Ligand field strength of the nitrogen end of cyanide and structures of cubic cyanide polymers. *Inorg. Chem.* **1965**, *4*, 725–730. [CrossRef]
68. Ng, C.W.; Ding, J.; Shi, Y.; Gan, L.M. Structure and magnetic properties of copper(II) hexacyanoferrate(III) compound. *J. Phys. Chem. Solids* **2001**, *62*, 767–775. [CrossRef]
69. Ojwang, D.O.; Grins, J.; Wardecki, D.; Valvo, M.; Renman, V.; Häggström, L.; Ericsson, T.; Gustafsson, T.; Mahmoud, A.; Hermann, R.P.; et al. Structure characterization and properties of K-containing copper hexacyanoferrate. *Inorg. Chem.* **2016**, *55*, 5924–5934. [CrossRef]
70. Avila, M.; Reguera, L.; Rodríguez-Hernández, J.; Balmaseda, J.; Reguera, E. Porous framework of $T_2[Fe(CN)_6] \cdot xH_2O$ with T = Co, Ni, Cu, Zn and H_2 storage. *J. Solid State Chem.* **2008**, *181*, 2899–2907. [CrossRef]
71. Sebastian, J.; Srinivas, D. Effects of method of preparation on catalytic activity of Co-Zn double-metal cyanide catalysts for copolymerization of CO_2 and epoxide. *Appl. Catal. A Gen.* **2014**, *482*, 300–308. [CrossRef]
72. Reguera, E.; Fernández-Bertrán, J.; Balmaseda, J. The existence of ferrous ferricyanide. *Transit. Met. Chem.* **1999**, *24*, 648–654. [CrossRef]
73. Fluck, E.; Kerler, W.; Neuwirth, W. The Mössbauer effect and its significance in chemistry. *Angew. Chem. Int. Ed.* **1963**, *2*, 277–287. [CrossRef]
74. Ito, A.; Suenaga, M.; Ono, K. Mössbauer study of soluble Prussian blue, insoluble Prussian blue and Turnbull's blue. *J. Chem. Phys.* **1968**, *48*, 3597–3599. [CrossRef]
75. Amr El-Sayed, M.F.; Sheline, R.K. The position of the C≡N stretching frequency in organic and inorganic molecules. *J. Inorg. Nucl. Chem.* **1958**, *6*, 187–193. [CrossRef]
76. Li, K.; Xue, D. Estimation of electronegativity values of elements in different valence states. *J. Phys. Chem. A* **2006**, *110*, 11332–11337. [CrossRef]
77. Mullica, D.F.; Milligan, W.O.; Beall, G.W.; Reeves, W.L. Crystal structure of $Zn_3[Co(CN)_6]_2 \cdot 12H_2O$. *Acta Cryst. B* **1978**, *34*, 3558–3561. [CrossRef]
78. Scherrer, P. Bestimmung der grösse und der inneren struktur von kolloidteilchen mittels röntgenstrahlen. *Nachr. Ges. Wiss. Gottingen Math. Phys. Kl.* **1918**, *2*, 98–100.
79. Williamson, G.K.; Hall, W.H. X-ray line broadening from filed aluminium and wolfram. *Acta Metall.* **1953**, *1*, 22–31. [CrossRef]
80. Roque, J.; Reguera, E.; Balmaseda, J.; Rodríguez-Hernández, J.; Reguera, L.; del Castillo, L.F. Porous hexacyanocobaltates(III): Role of the metal on the framework properties. *Microporous Mesoporous Mater.* **2007**, *103*, 57–71. [CrossRef]
81. Huang, Y.J.; Qi, G.R.; Chen, L.S. Effects of morphology and compositions on catalytic performance of double metal cyanide complex catalyst. *Appl. Catal. A* **2003**, *240*, 263–271. [CrossRef]
82. Nandan, B.; Venugopal, B.; Amirthapandian, S.; Panigrahi, B.K.; Thangadurai, P. Effect of Pd ion doping in the band gap of SnO_2 nanoparticles: Structural and optical studies. *J. Nanopart. Res.* **2013**, *15*, 1–11. [CrossRef]
83. Rouquerol, J.; Llewellyn, P.; Rouquerol, F. Is the BET equation applicable to microporous adsorbents? *Stud. Surf. Sci. Catal.* **2007**, *160*, 49–56.
84. Lippens, B.C.; Boer, J.H. Studies on pore systems in catalysts V. The t method. *J. Catal.* **1965**, *4*, 319–323. [CrossRef]
85. Dubinin, M.M. Physical adsorption of gases and vapors in micropores. In *Progress in Surface Science and Membrane Science*, 1st ed.; Cadenheat, D.A., Ed.; Academic Press: New York, NY, USA, 1975.
86. Balmaseda, J.; Reguera, E.; Rodríguez-Hernández, J.; Reguera, L.; Autie, M. Behavior of transition metals ferricyanides as microporous materials. *Microporous Mesoporous Mater.* **2006**, *26*, 222–236. [CrossRef]

87. Márquez, C.; Rivera-Torrente, M.; Paalanen, P.P.; Weckhuysen, B.M.; Cirujano, F.G.; De Vos, D.; De Baerdemaeker, T. Increasing the abailability of active sites in Zn-Co double metal cyanides by dispersion onto a SiO_2 support. *J. Catal.* **2017**, *354*, 92–99. [CrossRef]
88. Sreeprasanth, P.S.; Srivastava, R.; Srinivas, D.; Ratnasamy, P. Hydrophobic, solid acid catalysts for production of biofuels and lubricants. *Appl. Catal. A Gen.* **2006**, *314*, 148–159. [CrossRef]
89. Jadhav, A.R.; Bandal, H.A.; Kim, H. Synthesis of substituted amines: Catalytic reductive amonation of carbonyl compounds using Lewis acid Zn-Co-double metal cyanide/polymethylhydrosiloxane. *Chem. Eng. J.* **2016**, *295*, 376–383. [CrossRef]
90. Chen, C.; Cai, L.X.; Tan, B.; Zhang, Y.J.; Yang, X.D.; Zhang, J. Ammonia detection by using flexible Lewis acidic sites in luminescent porous frameworks constructed from a bipyridinium derivative. *Chem. Commun.* **2015**, *51*, 8189–8192. [CrossRef]
91. Chen, S.; Xiao, Z.; Ma, M. Copolymerization of carbon dioxide and epoxides with a novel effective Zn-Ni double-metal cyanide complex. *Appl. Polym. Sci.* **2008**, *107*, 3871–3877. [CrossRef]
92. Kember, M.; Kabir, R.; Williams, C.K. Method for Preparing Polyols. U.S. Patent 0,148,539A1, 2018.
93. Huang, Y.J.; Zhang, X.H.; Hua, Z.J.; Chen, S.L.; Qi, G.R. Ring-opening polymerization of propylene oxide catalyzed by a calcium-chloride-modified zinc-cobalt double metal-cyanide complex. *Macromol. Chem. Phys.* **2010**, *211*, 1229–1237. [CrossRef]
94. Kim, I.; Ahn, J.T.; Ha, C.S.; Yang, C.S.; Park, I. Polymerization of propylene oxide by using double metal cyanide catalysts and the application to polyurethane elastomer. *Polymer* **2003**, *44*, 3417–3428. [CrossRef]
95. Coates, G.W.; Moore, D.R. Discrete metal-based catalysts for the copolymerization of CO_2 and epoxides: Discovery, reactivity, optimization and mechanism. *Angew. Chem. Int. Ed.* **2004**, *43*, 6618–6639. [CrossRef]
96. Kobayashi, M.; Inoue, S.; Tsuruta, T. Copolymerization of carbon dioxide and epoxide by he dialkylzinc-carboxylic acid system. *J. Polym. Sci. Polym. Chem. Ed.* **1973**, *11*, 2383–2385. [CrossRef]
97. Eberhardt, R.; Allmendinger, M.; Zintl, M.; Troll, C.; Luinstra, G.A.; Rieger, B. New zinc dicarboxylate catalysts for the CO2/Propylene oxide copolymerization reaction: Activity enhancement through Zn(II)-ethylsulfinate initiating groups. *Macromol. Chem. Phys.* **2004**, *205*, 42–47. [CrossRef]
98. Kim, J.S.; Ree, M.; Shin, T.J.; Han, O.H.; Cho, S.J.; Hwang, Y.T.; Bae, J.Y.; Lee, J.M.; Ryoo, R.; Kim, H. X-ray absorption and NMR spectroscopic investigations of zinc glutarates prepared from various zinc sources and their catalytic activities in the copolymerization of carbon dioxide and propylene oxide. *J. Catal.* **2003**, *218*, 209–219. [CrossRef]
99. Ree, M.; Bae, J.Y.; Hung, J.H.; Shin, T.J. A new copolymerization process leading to poly(propylene carbonate) with a highly enhanced yield from carbon dioxide and propylene oxide. *J. Polym. Sci. A Polym. Chem.* **1999**, *37*, 1863–1876. [CrossRef]
100. Hsu, T.J.; Tan, C.S. Synthesis of polyethercarbonate from carbon dioxide and cyclohexene oxide by yttrium-metal coordination catalyst. *Polymer* **2001**, *42*, 5143–5150. [CrossRef]
101. Shen, Z.; Chen, X.; Zhang, Y. New catalytic systems for the fixation of carbon dioxide, 2. Synthesis of high molecular weight epichlorohydrin/carbon dioxide copolymer with rare earth phosphonates/triisobutyl-aluminium systems. *Macromol. Chem. Phys.* **1994**, *195*, 2003–2011. [CrossRef]
102. Chen, X.; Shen, Z.; Zhang, Y. New catalytic systems for the fixation of carbon dioxide. 1. Copolymerization of carbon dioxide and propylene oxide with new rare-earth catalysts-RE(P204)3-Al(i-Bu)3-R(OH)n. *Macromolecules* **1991**, *24*, 5305–5308. [CrossRef]
103. Li, Z.; Qin, Y.; Zhao, X.; Wang, F.; Zhang, S.; Wang, X. Synthesis and stabilization of high-molecular-weight poly(propylene carbonate) from Zn-Co-based double metal cyanide catalyst. *Eur. Polym. J.* **2011**, *47*, 2152–2157. [CrossRef]
104. Chen, S.; Zhang, P.; Chen, L. Fe/Zn double metal cyanide (DMC) catalyzed ring-opening polymerization of propylene oxide: Part 3. Synthesis of DMC catalysts. *Prog. Org. Coat.* **2004**, *50*, 269–272. [CrossRef]
105. Sun, X.; Zhang, X.; Chen, S.; Du, B.; Wang, Q.; Fan, Z.; Qi, G. One-pot terpolymerization of CO_2, cyclohexene oxide and maleic anhydride using a highly active heterogeneous double metal cyanide complex catalyst. *Polymer* **2010**, *51*, 5719–5725. [CrossRef]
106. Zhang, X.; Wei, R.; Sun, X.; Zhang, J.; Du, B.; Fan, Z.; Qi, G. Selective copolymerization of carbon dioxide with propylene oxide catalyzed by a nanolamellar double metal cyanide complex catalyst at low polymerization temperatures. *Polymer* **2011**, *52*, 5494–5502. [CrossRef]